Structural matters in HTSC: the origin and form of stripe organization and checkerboarding

2006 J. Phys.: Condens. Matter 18 R69

(http://iopscience.iop.org/0953-8984/18/6/R02)

INSTITUTE OF PHYSICS PUBLISHING JOURNAL OF PHYSICS: CONDENSED MATTER

J. Phys.: Condens. Matter **18** (2006) R69–R99 doi:10.1088/0953-8984/18/6/R02

TOPICAL REVIEW

Structural matters in HTSC: the origin and form of stripe organization and checkerboarding

John A Wilson

H H Wills Physics Laboratory, University of Bristol, Bristol BS8 1TL, UK

E-mail: john.a.wilson@bris.ac.uk

Received 29 June 2005, in final form 25 November 2005
Published 23 January 2006
Online at stacks.iop.org/JPhysCM/18/R69

Abstract

The paper deals with the controversial charge and spin self-organization phenomena in the HTSC cuprates, of which neutron, x-ray, STM and ARPES experiments give complementary, sometimes apparently contradictory glimpses. The examination has been set in the context of the boson–fermion, negative-U understanding of HTSC advocated over many years by the author.

Stripe models are developed which are 2-q in nature and diagonal in form. For such a geometry to be compatible with the data rests upon both the spin and charge arrays being face-centred. Various special doping concentrations are closely looked at, in particular $p = 0.1836$ or $9/49$, which is associated with the maximization of the superconducting condensation energy and the termination of the pseudogap regime. The stripe models are dictated by real space organization of the holes, whereas the dispersionless checkerboarding is interpreted in terms of correlation driven collapse of normal Fermi surface behaviour and response functions. The incommensurate spin diffraction below the 'resonance energy' is seen as in no way expressing spin-wave physics or Fermi surface nesting, but is driven by charge and strain (Jahn–Teller) considerations, and it stands virtually without dispersion. The apparent dispersion comes from the downward dispersion of the resonance peak, and the growth of a further incoherent commensurate peak pursuant upon the falling level of charge stripe organization under excitation.

Contents

1. Introduction

I have for a long time been trying to get the HTSC community to focus on a mixed-valent, two-subsystem, negative-U approach to cuprate superconductivity [1]. This has entailed going through the entire panoply of highly relevant data, whether the NMR and μSR data, or the laser pump–probe and thermomodulation optical data, or transport data such as the recent Nernst work, or once more the specific heat data. From the beginning I have advocated that the HTSC systems are electronically inhomogeneous, and have striven to show what it is that makes the mixed-valent cuprates unique within the Periodic Table, in addition to inserting further matters of 'chemistry' such as disproportionation, the Jahn–Teller effect, and the role of the ionicity of the various counter-ions used in these materials. The present work proceeds along comparable lines and readdresses the details of charge stripe behaviour, treated now on a diagonal 2-q basis. Both the hole-charge array and the attendant discommensurate antiferromagnetic spin array emerge alike as being face-centred, which accounts for the diffraction generated from these incipient orderings being as detected in synchrotron x-ray and neutron work. Sections 2 and 3 introduce and develop some of the topics necessary for addressing this matter appropriately, such as inhomogeneity, ionicity and p/d mixing, the spin and charge gapping and pseudogapping, structural adjustments and lattice coupling. The important aspect of the synchrotron radiation work in directly revealing charge ordering is emphasized, and

the results are correlated with those obtained for the nickelates. The difference between 1-q and 2-q incommensurate behaviour is highlighted. Section 4 looks specifically at the ordering encountered at key doping levels, and compares in particular the situation for $p = 0.157$, where T_c maximizes, with that for $p = 0.184$, where the superconducting condensation energy maximizes sharply. What is happening at these various special compositions is related through to the boson–fermion negative-U modelling advanced over many years by the author. Next addressed in section 5.1 is the new checkerboarding phenomenon, interpreted here in terms of correlation-driven Fermi surface 'boxing and unzippering' in the region of the extended saddles. In section 5.2 it is argued that the reported incommensurate (IC) magnetic behaviour likewise does not issue in the HTSC cuprates from standard Fermi surface nesting-dictated physics. Throughout the strong input of the axial saddles close to E_F is evident, and the latter clearly act to the overall benefit of HTSC rather than to its detriment.

Postscript, November 2005. At the request of the editors a short resumé is appended below of the nature and origin of the negative-U modelling employed here and developed in my earlier work on HTSC [1].

In highly correlated systems like the mixed-valent cuprates, just freed from Mott confinement, it might seem very odd to go forward with a negative effective Hubbard U value of -3 eV, rather than with some positive value $\sim+4$ eV (or $8t$) much as holds for the corresponding nickelates. This distinction is seen as arising from the circumstances, unique to the cuprates, of their terminal location in the 3d transition metal (TM) sequence. Double-loading fluctuations onto trivalent cuprate coordination units should not be 'projected out' of the problem, because they yield a shell-filling p^6d^{10} local electron count, which secures termination of $\sigma\sigma^*$ interaction between the relevant copper $d_{x^2-y^2}$ and oxygen $p_{x,y}$ states. These states experience with the excitation a total reorganization of their energies, that witnesses the p states rise and the d states fall dramatically, in particular in locally trivalent surroundings. Conditions in these mixed-valent materials remain sufficiently tight-binding and inhomogeneous (see the NMR and STM results) for local Coulombic forces and lattice relaxations (in part associated with the Jahn–Teller effect) to permit the key fluctuational state (represented by $^{10}Cu^{2-}_{III}$) to acquire a final energy virtually degenerate with the Fermi energy/chemical potential. The small binding energy of this state ($\sim$50 meV), as evidenced through neutron, Raman and EELS work, sizes the very large '$-U_{eff}$' as -3 eV, coming with the above relaxation. This effective 'reentrance' energy of -3 eV per pair (or $-1\frac{1}{2}$ eV per electron) in relation to zero ($^8Cu^0_{III}$) and single-loading ($^9Cu^{1-}_{III}$) is supported by a wide variety of optical measurements (see [1d, 1e]). Appearing in this regard very recently comes the spectral weight study from van der Marel and co-workers ((2005 *Phys. Rev.* B **72** 144503) and private communication), exhibiting spectral weight transfer near and below T_c into the low frequency region of the spectrum from the interband region up to 1.6 eV. Such increase in spectral weight in the low frequency intra-conduction-band range runs directly counter to standard BCS analysis; it signifies increase in stability in the condensed state via the band kinetic energy. This outcome, however, is in alignment with being at the BCS–Bose Einstein crossover within an attractive Hubbard circumstance, as is demonstrated by Toschi, Capone and Castellani in an even more recent release (2005 *Preprint* cond-mat/0509188) engaging dynamic mean field theory. This same crossover regime has been the subject too of a recent review by Chen, Stajic and Levin (2005 *Preprint* cond-mat/0508603), special emphasis being placed on the pseudogap region and the Nernst effect data just above T_c. As yet neither theoretical paper properly incorporates the inhomogeneity of the mixed-valent environment. The latter (and indeed its dynamically striped character examined in the present paper) is well manifested in the very recent ^{17}O NMR paper on $(La/Eu/Sr)_2CuO_4$ from Grafe, Curro, Hucker and Buchner (2005 *Preprint* cond-mat/0511408). Plainly the non-uniformity contributes much to the ARPES revealed break-up

of the Fermi surface in these materials. The latter matter has been treated formally by Civelli and co-workers by the cluster dynamic mean field technique (2005 *Phys. Rev. Lett.* **95** 106402). The doping disrupted four-site square plaquet they employ for the embedding process is very relevant to RVB and spin quenching, but clearly our current work calls for something a little more ambitious. The cluster pointed to below for closer examination has direct bearing on the standard objection made concerning negative-U-based superconductivity; namely that it leads to s-wave coupling. However, the latter is only so in the BCS limit, when proceeding with a (time-retarded) delta-function pairing potential. As was shown by Quintanilla and Gyorffy [67] this problem vanishes when one generalizes to a finite-range potential box. That change, coupled to a realistic band structure, witnesses $d_{x^2-y^2}$ become the natural symmetry outcome for these square-planar cuprate structures. The determined range of just $\sqrt{5}\,a_0$ is most appropriate to the present short coherence length, high T_c situation. The special position of copper within the Periodic Table is again crucial here, the heavy p/d mixing met with allowing expansion of the pair interaction to run over the bounding oxygens of the pair production centres.

I continue to find it really baffling why progress in this direction has been so long and vehemently resisted.

The present paper first appeared as 2005 *Preprint* cond-mat/0502666.

2. The electronic setting of local pair superconductivity in the cuprates

2.1. Concerning structural responses to electronic counts, shell closure and negative-U states

I would like to begin the present paper by commenting on that simplest of matters, namely the lattice parameters, and on what these are able to disclose about the HTSC condition. Recently Röhler has assembled [2] an extensive collection of high resolution crystallographic data taken from a diverse set of HTSC systems and has presented them in a form offering remarkably direct insight into what is afoot in these materials. Rather than plotting the lattice parameters a, b and c individually as a function of composition, Röhler has sought to avoid the various complications associated with the Jahn–Teller effect, octahedral tilting, c-axis charge reservoir effects, etc, by concentrating on the basal area of the CuO_2 planar unit, $B(p)$. The very striking observation to be gained from Röhler's presentation of the crystallographic data is that across the central superconducting range ($p \sim 0.10$ to 0.22), $B(p)$ always is in clear excess of what simple extrapolation in from the outer wings of the data plots would yield. This *upward* deviation of the data within the central region strikingly mimics the well known rise and fall of T_c, $B(p)$ similarly peaking near $p \sim 0.16$. What is more, between the various different HTSC systems the magnitudes of these $B(p)$ humps reflect the differing magnitudes of T_c^{opt}. Note that the above correlations are abstracted from *room* temperature data.

The decrease of lattice parameter witnessed from La_2ZnO_4 to La_2CuO_4 to La_2NiO_4 issues from the progressive fall from 2 to 1 to 0 in the occupancy of the *anti*bonding σ^* Cu(3d)–O(2p) e_g band of $d_{x^2-y^2}$ symmetry. These three occupancies are associated respectively with the formal divalent cation configurations d^{10}, d^9, and d^8, or, using my own preferred expanded notation introduced in [1a, 1b], $^{10}Zn^0_{II}$, $^9Cu^0_{II}$, and $^8Ni^0_{II}$. In cases where such a reduction in the number of σ^* electrons within the system actually is procured via increase in the average valence of a given TM element, as with the '*hole*-doped' mixed-valent cuprates, the ensuing decrease in the lattice parameters becomes even more pronounced, due to the covalent action of the bonding term now being augmented by an ionic one. Thus in LSCO $B(p)$ falls from 14.36 $Å^2$ at $p = 0.07$ to 14.18 $Å^2$ at $p = 0.30$, a drop of $1\frac{1}{4}\%$ [2]. It is this to be expected decline in $B(p)$ which now is demonstrated in the system holding the highest T_c dealt with

by Röhler—namely Hg-1212—actually to become completely negated over the central key range $p = 0.12$–0.21, prior to staging precipitous recovery of the anticipated behaviour beyond $p \approx 0.24$.

Our earlier work encourages one to view this hump found in $B(p)$ as the product of a local pair bosonic population, the latter acquired in fluctuational style within a system that displays near-resonance between the quasiparticle Fermi energy and the local-pair ground-state [1]. Here the pair involved is, note, a two-electron one, not a two-hole one as is customarily presumed by others [3, 4]. In our previous treatment [1b] the above key bosonic fluctuation has been designated $^{10}Cu^{2-}_{III}$. This transient two-electron cell loading becomes sensed in the crystallographic work by virtue of the locally generated p^6d^{10} count. Such shell filling fully negates all p/d bonding within the trivalent coordination unit taking on the two additional electrons and relaxes the bond length. For the customary two-*hole* boson state one conversely would find a decrease in lattice parameter (i.e. see a dip in $B(p)$) as one acquires a local condition in which the individual polaronic hole carriers (site hybridized $^8Cu^0_{III}/^8Cu^{1+}_{II}$) become bound together into pairs as two-site bipolarons [5].

2.2. Concerning highly local, inhomogeneous electronic behaviour

That the above mixed-valent substitution in the HTSC cuprates generates significant inhomogeneous electronic behaviour at the atomic level is today surely incontestable. Improved analyses of the NMR [6] and μSR [7] data, plus the remarkably graphic energy-resolved scanning tunnelling microscope results [8], all clearly register the high degree of local disturbance and intrinsic local variability experienced in these systems to beyond optimal doping. Indeed it is not really justified to contemplate using mean-field approaches and standard Fermi liquid theory until one has passed entirely beyond the superconducting range. The most basic of transport measurements serve to show the chronic level of scattering experienced by the charge carriers right across the range, and from which not even the nodal carriers are immune [1c, 9]. The Seebeck coefficient, for example, makes very evident the persisting degree of development of a density-of-states pseudogap even as T_c maximizes [10]. Indeed the very fact that the carriers respond at low temperatures as holes throughout the HTSC range makes clear how far correlation and site disorder are pushing the systems to a localized condition. This observed hole character in the II/III cuprates is despite having E_F sited within the *lower* half of what standard LDA band structure calculations would present as an effectively sinusoidal 2D band, the latter supporting an almost circular Fermi surface. ARPES results [11] provide a clear record of the progressive disintegration of Fermi liquid behaviour upon reduction in the dopant concentration, as one withdraws towards the properties of the undoped parent d^9 Mott insulator. Accordingly it would seem quite inappropriate to appeal to rather simple Fermi liquid nesting physics when attempting to interpret, for example, the magnetic behaviour of HTSC materials. The superconductivity itself, indeed, makes apparent the local character of these materials in its coherence lengths, ξ, of just three or four unit cells [12].

2.3. Concerning hole concentration dependence of pair density, condensation energy and T_c

Complementary to the short coherence lengths of HTSC materials come their long penetration depths, λ. λ may readily be extracted from μSR data [13], and these provide then a direct monitor of the superconducting pair concentration, n_s ($\propto \lambda^{-2}$). Most significantly this pair population is dictated by the '*hole*' dopant concentration p ($n_s = p/2$) over quite an extensive range, and not by the complementary electron count, $1 - p$. Even more revelatory of HTSC behaviour is that, once clear of the superconducting onset around $p = 0.05$ [14], T_c is found

to rise steadily tracking $n_s(p)$ up to about $p = 0.125$ [15]. Beyond the latter doping level, first $T_c(p)$ comes slowly to a maximum—this universally at $p = 0.16$ according to the empirical findings of Tallon *et al* [16]—to be followed shortly thereafter near $p = 0.185$ by $n_s(p)$ as well. The strong fall back in $n_s(p)$ that follows upon yet further increase in p has become known as the 'boomerang' effect. This can most fully be observed in the Tl-2201 system, which is subject to high overdoping in consequence of its complex defect structure [16]. The effect does not result from a decrease in m^* which should carry the μSR signal in the opposite direction. The above turning points in $T_c(p)$ and shortly thereafter in $n_s(p)$ arise naturally within the resonant boson–fermion (B–F) modelling of HTSC [1].

From the analysis of the electronic specific heat work presented by Loram *et al* [17], one may witness an effect directly related to the above; namely of having $T_c(p)^{max}$ arrive slightly in advance of the concentration p ($\sim$0.185) at which $U_c(p)$, the superconducting condensation energy per gram-atom, mounts sharply to its maximum. Here $T_c(p)$ is more a monitor of the effective pairing strength, whereas $U_c(p)$ tracks the progress of the entire condensation, not just condensed local pairs, but also those additional quasiparticles being brought into Cooper pairing under the resonant action of the local pairs [1, 18–20]. At the stage where T_c maximizes ($p \approx 0.16$), the HTSC cuprates still show a fair degree of pair breaking coming from the level of remnant magnetism [7, 21]. This capacity for pair breaking is, however, dropping away very rapidly with p, and the most effective composition for gaining maximization of n_s and U_c is delayed only fractionally behind that for T_c. The reason why T_c universally optimizes near $p = 0.16$ is that this value constitutes a particular geometrical criterion in the interrelation between the two subsystems existing within the square-planar, mixed-valent materials in regard to electronic microstructure and percolation [1i].

2.4. Concerning boson–fermion resonance, ionicity, Jahn–Teller effect, pair breaking and spin gap

To achieve optimization of T_c between the *different* HTSC systems calls for (i) reaching the resonance between the local pair negative-U state and the chemical potential at precisely the above critical p value, and (ii) having the magnetic pair breaking in the system at this point as low as is feasible, so limiting the delay in the peaking of $n_s(p)$ and $U_c(p)$ *vis-à-vis* $T_c(p)$. For HTSC systems the way to suppress the pair-breaking capacity is to increase the general covalence. Towards this end one may pursue two different courses [1f, 1g]: (i) introduce counter-ions into the system of high atomic number, such as Hg, Tl, Pb, and Bi, thereby augmenting the overall dielectric constant and screening, and (ii) generate chemical pressure within the basal plane by enhancing the Jahn–Teller distortion of the $^9Cu^0_{II}$ divalent subsystem. It is found that mercury secures the best results here. Indeed the Jahn–Teller distortions in the mercury cuprates reach quite exceptional values—for the case of Hg-1201, basal and apical Cu–O bond lengths of 1.94 Å versus 2.80 Å, respectively. What the Jahn–Teller deformation of the Cu–O coordination unit secures is compression of the CuO_2 basal plane, via added stabilization of the $d_{x^2-y^2}$ symmetry bonding σd/p band and destabilization of its partially occupied σ^* counterpart relative to the full d_{z^2} symmetry antibonding band. In the earlier of the 'higher order' HTSC systems this beneficial contraction in the crucial outermost CuO_2 planes (i.e. those proximate to the excess hole-introducing oxygen atoms) is augmented by the additional compacting action of the *four*-fold coordinate, inner planes. This process advances T_c up to such a stage order that magnetism reemerges within the now virtually undoped innermost layers. At optimal doping, a_o, the cell edge, from its value of 3.882 Å in Hg-1201, becomes 3.859 Å in Hg-1212, 3.852 Å in Hg-1223, and 3.850 Å in Hg-1234, while

the corresponding T_c^{max} values are 97, 127 and 135 K, but then 127 K, with a yet further fall to 110 K in Hg-1245 [22].

What specifically the above advance in covalence secures as regards pair breaking is a decrease in the effective magnetic moment formed at magnetically active sites [23], and the emergence of spin-singlet spin-gapping via promotion of dynamic RVB coupling [24] at the expense of frozen Néel order. The size of the spin gap accordingly is smallest in LBCO and LSCO [25] and rises through $YBa_2Cu_3O_{6+x}$ [26] to the more weakly ionic HTSC systems like Tl-2201 [27] and Bi-2212 [28]. One way to reverse the above development is, of course, to apply an external magnetic field [29, 30] (a subject we return to later). A more unexpected and revealing way to promote pair breaking is to substitute some of the Cu in the planes by Zn. The effect is locally to free up the spins around each substituent centre, this causing T_c to fall particularly rapidly. The process has been examined through μSR [31], transport [32], neutron scattering [33] and many other measurements. The p value offering the optimization of $T_c(p, y)$ becomes steadily forced up by the Zn substitution level, y, towards where $n_s(p)$ maximizes near $p = 0.185$, in order to gain relief from the severity of the pair breaking and a restoration of delocalization.

2.5. Concerning the tight-binding bandstructures, the level of p/d mixing and screening

$YBa_2Cu_3O_{6+x}$, although so widely studied, introduces added complication by virtue of the nature of its 'charge reservoir', the partially oxygenated Cu–O chains. This reservoir participates more intimately in events than is the case for most other HTSC systems. In particular the copper chain sublattice ultimately shares in the superconductivity, although the μSR results clearly reveal that the many paired carriers finally showing up in the chain regions of the structure do not contribute significantly towards advancing T_c [34]. Only the hole population transferred through from the reservoir onto the planes brings about the HTSC response. By $YBa_2Cu_3O_{7.0}$ the 123 system has become just slightly overdoped ($p \sim 0.17$) in the sense that T_c has just peaked. It is possible to advance the planar hole content even higher by making the counter-ion substitution of Ca^{2+} for Y^{3+}, and in this way to access the overdoped planar regime of falling T_c, n_s and U_c [35, 36, 17]. Independently the chains in the system are meanwhile free to display CDW behaviour [37], this of course as well as presenting a transverse structural ordering of their variable oxygen atom content [38].

Because $YBa_2Cu_3O_7$ itself is stoichiometric and relatively metallic, even a standard LDA band structure calculation is able to offer some useful insight into the electronic circumstances prevailing in general within mixed-valent HTSC systems. Such calculations reveal immediately the high degree of tight-binding and ionic behaviour current in all these oxides even at optimal doping. When the wavefunctions appertaining to the entire valence band are summed, the bulk of those electrons are indicated to reside in quasi-ionic, spherical distributions [39]. When only the particular wavefunctions present at E_F are summed, one furthermore can see how those electrons become distributed in real space. In YBCO-123 the two fuller of the three $d_{x^2-y^2}$ bands ($Z = 1$) locate their electrons primarily within the planes, whilst the third and much *emptier* $d_{x^2-y^2}$ band sites its electrons almost exclusively on the chains. This means the octahedral coordination units display the lower formal valence. There is clear register within these plots of the emergence of one sixth of a *hole* within each of the two latter Cu–O units per formula unit. The complementary one third of an electron coming through onto the chains (per Cu there) then sources the metallicity, the CDWs and the superconductivity appertaining to that segment of the structure [1f].

What such band structures and their associated charge plots make very apparent for the HTSC cuprates is the particularly high degree of p/d mixing. This mixing is due to the

imminent closure of the copper d-band and the already strongly descending (i.e. stabilizing) energy of all the d-subbands [1i, 40]. Within the hybridized p/d σ/σ^* manifold of states having $d_{x^2-y^2}$ symmetry, considerable oxygen p weighting has become 'inverted' from the fully occupied σ and into our partially occupied σ^* band. Even for a purely *divalent* cuprate the p/d admixing already is such that the upper partially occupied wavefunction of the σ^* band bearing E_F runs extensively over the oxygen as well as the copper sublattice; i.e. even at this ($^9Cu^0_{II}$) loading the p-shell is not exhibiting the closed p^6 condition. Note that this non-closure is not the product of E_F entering here the top of the non-bonding p_z band. In the case of a mixed-valent system undergoing augmentation of its average valence, the admixed d-states bear now proportionately even less of the introduced hole than do the already opened $p_{x,y}$-states. The quasiparticles in the cuprate II/III systems in fact run quite as freely over the oxygen sites as they do over the copper sites in the cell. One accordingly encounters far greater metallicity in these cuprates than is the case for the analogous nickelates and manganates. The great benefit of this freeing up of the spatial extent available to the relevant wavefunctions is that there occurs appreciable reduction in the coulombic repulsion between carriers from the much more effective screening.

The above advanced level of p/d mixing in the cuprates, and of how it adjusts to changes in the hole doping concentration, has very recently been directly evaluated by NMR, both for LSCO and for YBCO [41]. The latter data register very clearly how the fresh space opened up to conduction indeed runs largely over the oxygen sublattice. This fact reemphasizes why it is so important when designating the hole doping centres to employ Cu_{III} as preferred book-keeping device for the number of electrons in play, the symbol referring to the entire coordination unit, and to avoid as far as possible the frequently used symbols Cu^{3+} or d^8. All copper chemistry tells one that it is never possible to access anything like d^8Cu^{3+} outside a hard Mott insulator like $KCuF_4$ (see figure 3 in [1i]). This essential chemistry, resulting from the imminence of shell closure, is missed in much simple numerical modelling of the cuprates. The key outcomes to follow in HTSC materials are (i) the facilitating of p^6d^{10} two-electron shell-closure fluctuations and transient negative-U pair formation, and (ii) the restricting of local spin fluctuations and their pair-breaking action.

2.6. Concerning disproportionation and less extreme structural adjustments

The above situation relating to p/d mixing when extended to second and third TM series group VIIIc materials leads to full-blown static disproportionation in divalent AgO [42] or AuO and $CsAuCl_3$ [43]. By contrast for the first series *mixed-valent* II/III cuprate systems, the potential self-organization states are the somewhat less extreme ones of electronic stripe formation, of clustering, or, possibly, of its converse, Wigner crystallization. The latter options disturb less the underlying structure of the lattice. As has been noted earlier in section 2.1, a good deal of structural activity is, nevertheless, current right up to optimal doping, as is recorded under the local electronic probes of NMR [6], μSR [7], and energy-resolved STM [8], or again in the direct lattice probings afforded by the EXAFS [44], PDF (pair distribution function) [45] and DW (Debye–Waller) [46] techniques. What now are in question are the timescales and the degrees of self-ordering actually attained.

All HTSC systems display some tendency towards such electronic ordering around $p = \frac{1}{8}$ [47, 1e], and in fact this is statically acquired in LBCO [48, 49] with possible assistance from a slight structural adjustment in the tilting of the Cu–O octahedra. This structural change (from LTO to something akin to LTT) precedes by about 10 K the onset in LSCO of the detected electronic ordering. The latter ordering clearly has both magnetic and charge components to its character. Since all HTSC systems would appear to exhibit some susceptibility to a $\frac{1}{8}$th

event, and to what early neutron diffraction work suggested to involve stripe segregated charge and magnetic phase-slip, we shall examine more closely below just what current diffraction work, neutron and x-ray, indicates that incipient order might be. Any geometrical micro-ordering clearly is of much potential import towards understanding the details of HTSC. As has been alluded to already, the point where T_c universally maximizes is set by the geometric criterion of percolation, whilst the above $\frac{1}{8}$ anomaly would seem in LBCO and LSCO to pick up commensuration energy associated with the 'LTT' structuring. Finally it might be recalled that in high quality LBCO, when the $\frac{1}{8}$ anomaly structure actually becomes frozen in, it becomes associated with a total suppression of HTSC [50].

3. Experimental input into resolving 'stripe phase' structuring

3.1. Concerning charge stripe orientation and lattice coupling through the Jahn–Teller effect

Because in LBCO the $\frac{1}{8}$ structure actually freezes in, it is possible to investigate the frozen structure quite closely from existing neutron and x-ray data. Immediately it is evident from the relative elastic neutron scattering line-widths reported in [49] that the degree of magnetic organization ultimately developed is of a higher level than is the charge order. This matches the fact that the $^{9}Cu^{0}_{II}$ sites carrying the magnetic moments constitute the majority species. The moment-free minority $^{8}Cu^{0}_{III}$ species being more sparsely distributed are less strongly coupled. It has become commonplace to speak of such organization in terms of stripes as distinct from clustering, and, indeed, with the materials customarily being quenched from high growth temperatures, there is little evidence of any clustering of the substitutional counter-ions themselves. The maintenance of local charge neutrality indeed is against this. What drives the observed ordering in the mixed-valent cuprates would seem, as with the corresponding manganates and nickelates, to be the strain field associated with the strong Jahn–Teller activity in our σ/σ^* bands of e_g-related symmetry. Accordingly the detected ordering reflects more the adopted locations of the dopant 'holes' than it does the precise locations of the introduced ions. Within the LSCO and Hg-1201 structures the dopant ions are directly proximate to four Cu atoms in a checkerboard plane. As examination of figure 4 in [1i] will reveal, the electrons have little more to do then than to settle preferentially into one or other of those four coordination units to produce substantial organization along the above lines.

A quasi-linear response becomes the simplest way in which to effect self-organization of the excess charge and at the same time bound the magnetic moment bearing domains. Such organization is well-suited to canted runs of Jahn–Teller distorted $^{9}Cu^{0}_{II}$ octahedra, capable of accommodating to the more regularly shaped octahedra associated with the hole-bearing stripes, that remain untilted [51]. In the orthorhombic LTO structure of the pure divalent parent La_2CuO_4 itself, canting already occurs, with the canting axis running in one particular 45° direction (neglecting twinning). What happens in the much examined case of $p = \frac{1}{8}$ LBCO is that at the crystallographic transition near 60 K the unit cells revert from being uniformly orthorhombic to being on average tetragonal. This change introduces an averaged basic cell now precisely of $\sqrt{2}\times\sqrt{2}\ a_0$ (HTT), as the octahedral tilting of the LTO state fragments from occurring in uniform rows parallel to a *single* 45° axis (per orthorhombic domain)—first clockwise, then anticlockwise—into attempting to follow a more complex pattern of local site tilts about both diagonal axes. This passage from a single- to a two-axis condition is the structural forerunner of the charge and spin organization duly to emerge at slightly lower T within the *electronic* system in mixed-valent material. The above pattern of LTT tilts is such that the associated unit cells retain 45°-rotated form, and one might well anticipate that as the electronic stripes develop they follow these same, now fully equivalent, orientations.

3.2. 2-q versus 1-q behaviour and its influence on diffraction from discommensurations and stripes

Much as the double-axis tilts in the LTT structure above do not introduce a 2×2, x, y cell, so one has to be careful, when dealing with 2-q as distinct from 1-q incommensurate behaviour, not to rush to ascribe the predominantly x/y subsidiary spotting observed in the spin- and charge-organized diffraction patterns to features running in the x- and y-axis directions. When drawing up the figures in the appendix of [1f], or again in [1e], I was myself guilty of this mistake, and should not have been since we had long experience of stripe phase structures in more than one dimension. The latter arose in connection with the discommensuration arrays we had found in the incommensurate CDW phases of 2H-$TaSe_2$, etc. Figure 10 in [52a] or figure 2 in [52b] will serve to illustrate how, for the hexagonal geometry there, the discommensurations (DCs) align themselves at 30° to the incommensurate wavevectors of the diffraction pattern. This occurs as the DCs entail simultaneous phase-slips along more than one principal direction. In the square-planar cuprate case there is involved a π phase-slip in the $2a_0$ AF spin array along both the x- and y-axes, and this leads to overall magnetic pattern displacements of $\sqrt{2}a_0$ in the 45° directions. Fortunately the DC arrays that arise now in the symmetric 2-q tetragonal case are considerably simpler than those for the symmetric 3-q hexagonal case, where the three active IC vectors led to a 'double honeycomb' domain structure [52].

In the cuprate case there has so far been almost exclusive focus on 1-q striping, stemming from Yamada *et al*'s finding that the size of $\mathbf{q}'_{\mathrm{I}}$ is linearly proportional to p up to about $p = \frac{1}{8}$ [53, 1e]. Here the $\mathbf{q}'_{\mathrm{I}}$ are the four equivalent subsidiary wavevectors expressing the incommensurateness of the magnetic structuring away from the commensurate cell corner reference vector of the parent antiferromagnetic condition. In the $p = \frac{1}{8}$ case, $\mathbf{q}'_{\mathrm{I}}$ becomes $(\frac{1}{4}, 0)$, etc, when expressed in terms of the vector 'π, π' [or $(1/2, 1/2)2\pi/a_0$] of the Néel state of LCO (a_0 being for the $z = 2$ bct HTT structure). The relatively high intensity of these magnetic satellites is subsumed from the now defunct parent AF (solely spin-based) spotting. This magnetic scattering, elastic for LBCO $p = \frac{1}{8}$, is accompanied by its charge counterpart (much weaker in neutron scattering) at wavevectors $\mathbf{q}'_{\mathrm{I}}$ of $(\frac{1}{4}, 0)$, etc, where this time the latter IC spots have been quoted in relation to the basic lattice vector: i.e. in real space they are expressed in units of a_0 and not the $2a_0$ relevant to the antiferromagnetic spotting. Accordingly, here at $p = \frac{1}{8}$ the *axial* charge modulation period amounts to $4a_0$, whilst the accompanying *axial* spin modulation period is twice this at $8a_0$. The $\mathbf{a}^*_0/4$ charge spotting, whether it is sensed by neutrons or x-rays, is of extremely low intensity and it derives independently of the ions through the superlatticing diffraction of the holes themselves. $\mathbf{a}^*_0/8$ diffraction spotting from this organized charge array is, as we are to see later, forbidden by reason of the axially face-centred form to the ordering (see section 4.1).

3.3. Sources of electronic organization. Case of $(La_{2-x}Sr_x)NiO_4$. Magnetic order and pseudogapping

I would hesitate to call the above periodic entities CDWs and SDWs, because I have always tried to limit those terms to states with wavelengths dictated by the Fermi surface topology, as for certain layered transition metal dichalcogenides [54]. Personally I do not see this as being the case with the HTSC cuprates. As the ARPES results serve to highlight [11], the Fermi surface is not well established in the latter materials, especially around the saddles at low p. Furthermore, were nesting to be occurring across individual arms of the FS (as in the 1T dichalcogenides), the CDW wave*length* should grow with p, not the converse as observed experimentally [53]. Again, if the nesting were between pairs of saddle points, as seems the

case with 2H-$TaSe_2$, etc, the nesting vectors ought to be much closer to $\mathbf{a}_0^*$ than are the displayed $\mathbf{q}_I$. Finally, if the nesting were across the body of the zone, as many would claim, then the IC spots would define directly the principal vectors (as say in chromium), and not represent subsidiary ones—the $\mathbf{q}_I'$, associated above with discommensurate striping. We then would be relating the spotting to x, the full electronic count, rather than it pointedly monitoring the hole count p away from half filling. Any relatively standard RPA treatment of the susceptibility looks misplaced here in the light of Yamada *et al*'s telling observation, $|\mathbf{q}_I'| = p$ [53]. As I emphasized earlier in [1e, 1f], the latter relation speaks of some simple numerology within a real space dictated organization.

The latter type of direct interaction finds excellent illustration in the charge striping arrays recently to have been recorded in detail by Ghazi *et al* [55] in synchrotron x-ray work on the analogous $(La_{2-x}Sr_x)NiO_4$ system. With the latter, and for x and q_I between $\frac{1}{4}$ and $\frac{1}{3}$, cooling to helium temperatures reveals strong lock-in effects in the $\mathbf{q}_I$ to values of 0.294 and 0.313 $\mathbf{a}_0^*$, besides to 0.333 $\mathbf{a}_0^*$ itself (see their figure 10). It is to be noted that what these lock-in values amount to are $\frac{5}{17}$, $\frac{5}{16}$ and $\frac{5}{15}$ precisely. They arise here under discrete, five-bit, row sequencing in relation to segregated hole siting, depending on whether holes are confined to each third atom row or become delayed until a fourth, generating 17, 16 and 15 row sequences of respectively

$$\mathbf{3}\,4\,3\,3\,4\,\mathbf{3}, \quad \mathbf{4}\,3\,3\,3\,3\,\mathbf{4}, \quad \text{and, ultimately,} \quad \mathbf{3}\,3\,3\,3\,3\,\mathbf{3}.$$

We shall encounter later too $\frac{5}{18}$ or 0.278, this associated with **4** 3 4 4 3 **4**. The above form of faulting long has been known for defect compounds and alloys, e.g. $Cu_{2-x}Te$ and $Ni_{3-x}Te_2$ [56], and it normally has little to do with the fermiology: indeed it may occur in non-metals.

The level of local disturbance which the onset of charge stripe order itself creates amongst cells (dependent upon their individual proximity to the stripes) has numerically been assessed across a wide range of LSCO samples via an extensive PDF analysis undertaken by Billinge *et al* of their low temperature neutron scattering data [57]. Unfortunately in their modelling they presume uniaxial striping, but this should not invalidate their principal finding that the *spread* incurred in the distribution of local Cu–O basal bond lengths in fact is largest for x just slightly above 0.15. This spread has become 0.02 Å larger there than that present within the bounding, stripe-free systems $x \approx 0$ and 0.25. Such peaking in local disturbance to the structure (figure 3(a) in [57]), unlike the peaking introduced in our section 2.1 regarding the average lattice parameters across the same range of x, arises in the present case only once into the low temperature charge-ordered regime. It this time is the direct reflection of the stripe ordering and cannot issue solely under the disorganized mixed valence alone.

With neutron work the degree to which the stripe organization actually becomes apparent for a given HTSC system depends greatly upon the level there to which the magnetism remains unquenched (see section 2). Magnetic discommensurations are going to be readily discernible only in circumstances where RVB coupling has not been able to override residual Néel coupling. In $YBCO_7$ this limits the condition for seeing the $\mathbf{q}_I'$ striping spots to inelastic excitations above ∼33 meV [26] (≡400 K and locally equating to T_N in $YBCO_6$). For LSCO in the vicinity of $p = \frac{1}{8}$, the spin gap takes the much smaller value of about 7 meV [25], and indeed for LBCO it has become reduced to near zero, the superstructure actually freezing in [49]. As was noted previously, the spin gapping may be delayed by the application of a magnetic field [29, 30]—this inside any type II superconductor below T_c being quantized into flux vortices. Recent neutron work from Gilardi *et al* [58] on overdoped $x = 0.17$ LSCO has demonstrated that, under an external magnetic field of just 5 T, a sizeable residue of magnetic scattering, strong at 40 K just above T_c, persists now right down to 5 K even for excitation energies as low as 4 meV. In this work, $\mathbf{q}_I'$ itself was observed to have increased from the $\frac{1}{8}\mathbf{a}_0^*$

at $p = 0.125$ to $\frac{1}{7}\mathbf{a}_0^*$, a value earlier in evidence at 5 K in [25] when using a slightly overdoped $x = 0.165$ LSCO sample.

3.4. Using x-ray work to probe charge organization

Whilst most of the attention hitherto has been on neutron diffraction and the spin array, reflecting and indeed fostering a preoccupation with spin fluctuation modelling of HTSC, we now shall pay particular attention to the charge array information deriving from x-ray scattering. Because we are sensing there only the hole charge ordering, the resulting scattering intensity becomes extraordinarily weak and this calls for synchrotron work. Niemöller *et al* [59] have undertaken such work at DESY, and they published their findings in 1999 in what has proved a surprisingly little quoted paper. Their work on a $x = 0.15$ $(La, Nd, Sr)_2CuO_4$ sample contains, however, at least a dozen points of key importance towards resolving what is afoot:

(1) the $\mathbf{q}_1''$ charge spot intensity is only $\sim 10^{-8}$ that of the basic Bragg spots;
(2) the size of this wavevector is at $x = 0.15$ still connected with an $8a_0$ periodicity;
(3) the modulation coherence length, at 44 Å, stays similarly unchanged from what it was for $x = 0.125$. Note that the latter distance amounts to $\sqrt{2} \times 31$ Å, where 31 Å equals $8a_0$;
(4) the peak intensities are, however, 30% weaker at $x = 0.15$ than they were at $x = 0.125$;
(5) the above charge order coherence length proves to be temperature independent, and it is in this unlike the magnetic coherence length which decreases continuously with temperature increase;
(6) the amplitude of the charge order diffraction spots diminishes meanwhile approximately linearly with T;
(7) unlike in the $x = 0.125$ case, the charge order spotting for the $x = 0.15$ sample onsets on cooling only some 8 K below the LTO → LTT transition (this now at 62 K). The latter structural transition is monitored here by growth of the (3, 0, 0) Bragg spot, forbidden in the LTO structure;
(8) once away from $x = 0.125$, the charge ordering sets in, furthermore, at a somewhat *higher* temperature than does the spin ordering. This very significant observation was reported too in [48] by Tranquada *et al*;
(9) the charge order remains in evidence, what is more, down into the magnetic pseudogapping regime where magnetic spotting has faded away;
(10) for the $x = 0.125$ case, the charge and magnetic orderings appear simultaneously, triggered by the LTO → LTT structural transition;
(11) once below $x = 0.125$, charge ordering persists up through into the LTO condition, far above T_c, a circumstance evident too in the Cu NQR work from Hunt *et al* [60];
(12) the level of charge ordering is sufficiently strong that there exists clear z-axis correlation: the main superspotting develops at $0.5\ \mathbf{c}_0^*$, appropriate to a four-layer stacking sequence.

From this and the preceding introduction we now have gathered enough data to construct geometrical models for the observed charge and spin structuring as a function of p.

4. The structural setting of local pair superconductivity in the cuprates

A series of stripe organized structures will be presented below, constructed in compliance with the foregoing experimental input and understanding. These identify the key p values within the HTSC phenomenology: namely (i) $p = 0.125$ (or $\frac{8}{8^2}$), where the stripe organization is strongest, and manifestly acts there to the detriment of HTSC; (ii) $p = 0.1563$ (or $\frac{10}{8^2}$),

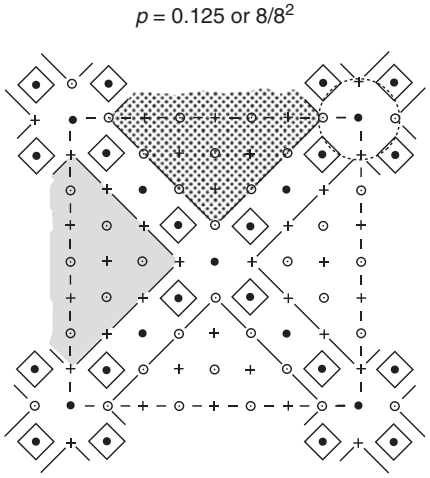

Figure 1. Diagonal stripe array for $p = 0.125$. Coordination units bearing a hole charge are emphasized. Spins at the Cu_{II} sites in the magnetic domains are nominally labelled 'up' ($\odot$) and 'down' (+). The array is face-centred with regard both to its hole content and also to its 45° rotated magnetic domaining, as indicated by the shading. The charge stripes (enclosed by diagonal lines) form between the antiferromagnetically ordered spin domains, and fall where the latter exhibit a_0 ($\pi-$) phase slippage in the AFM. This slippage occurs simultaneously in both the x and y directions to generate discommensurations in the spin array which follow the 45° orientation of the charge stripes. Within the latter the charge holes alternate with non-magnetic Cu_{II} sites. Note that the face-centred arrangement of the antiferromagnetic domains is what causes the neutron spin diffraction to produce no diagonal spotting. Here at $p = \frac{1}{8}$ is the most concentrated hole array for which the simple Yamada relation $|\mathbf{q}'_{I}| = p$ holds.

where T_c maximizes; (iii) $p = 0.1837$ (or $\frac{9}{7^2}$), where the condensation energy per pair, $U_c(p)$, maximizes; (iv) $p = 0.277$ (or $\frac{10}{6^2}$), where superconductivity terminates, and (v) $p = 0.055$ (or $\frac{22}{20^2}$), where HTSC commences.

4.1. $p = 0.125$ or $\frac{8}{8^2}$ (see figures 1–3). Charge stripes and magnetic discommensurations

The $8a_0$ cell in figure 1 is the one for which, as we have seen, most data exists, the stripes/DCs being there frozen in, or nearly so, and the diffraction sharp. The domains of antiferromagnetically coupled spins stand in antiphase across the DCs, these shown aligned in the 45° orientations. The magnetic spotting implies a full two-atom phase-slip of the 'up/down' $2a_o$ spin sequence, due after four such units, i.e. $8a_0$, or, rather, in the present case, a registerable 180° phase-slip of a_0 after just two such units, i.e. $4a_0$. In the latter case, at a general x coordinate in the cell, upon moving in the y direction in figure 1 we traverse then two what might be termed 'partial discommensurations' within the supercell repeat of $8a_0$. At those x values corresponding to the DC crossing-points a y-axis traverse witnesses the action of the pair of DCs becoming fused into a single 360° phase-slip.

The domains magnetically are not all equivalent but fall into two sets, 'up'-centred and 'down'-centred. The true orientation of the spins remains in fact undetermined. Some suggest that the spins lie in or very close to the basal planes [61], as in La_2CuO_4 itself [62], whilst others favour a c-axis orientation. The real circumstance doubtless is more complex. It is hard to imagine that the bounding charge stripes are not going to affect the anisotropy forces which locally constrain the spin orientations. Probably the stripes also affect the local spin

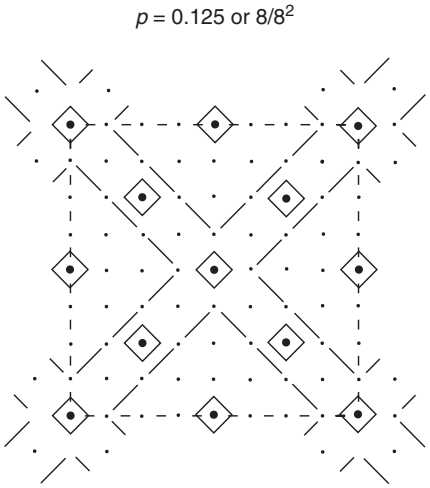

Figure 2. The figure shows what would amount to Wigner crystallization of the dopant charge at $p = \frac{1}{8}$. Hole charge has been shifted within the stripes of the previous figure to occupy the cell centre and corner sites where the stripes cross. The 'surplus' holes then have been reinserted at the domain centres. This disperses the hole charges as widely as possible. It is not what occurs in the cuprates.

magnitudes. Recall μSR experiments [7, 23] indicate a 50% drop in the *average* moment from the 0.6 μ_B of the parent $p = 0$ Mott insulator, and they reveal a very considerable spread in local μ values. Of course this spread is much contributed to by what exists inside the stripes. As drawn in figure 1, there are, per $8a_0$ cell of 64 units, 26 coordination units fully within the domains; 24 sit on their boundaries and the remaining 14 are located inside the stripes. The holes in these stripes alternate with moment-quenched Cu_{II} sites, so enabling us to arrive at the perceived requirement $p = |\mathbf{q}'_I|$ at this one-eighth doping level. Note that the magnetic domain periodicity along the 45° direction becomes $\sqrt{2} \times 8a_0$, or 44 Å, the observed low temperature spin modulation coherence length. In particular, note too the face-centring character to the above discommensurate array of 45°-rotated antiferromagnetic square domains, highlighted via the shading. This is the origin of the experimental absence of magnetic spotting in the 45° orientations.

If the phasing *along* a charge stripe above were to be slipped so that the stripe crossing point now becomes a hole, the dopant count per $8a_0$ cell would decrease from $\frac{8}{8^2}$ to $\frac{6}{8^2}$, which then would not fulfil the Yamada requirement $p\ (=n_h/A) = |\mathbf{q}'_I|$. However, if the two dopant holes so shed are now returned symmetrically to the $8a_0$ cell, at its domain centres, we arrive at the situation portrayed in figure 2. The structure reached here is the one for which the hole population stands maximally dispersed. It represents Wigner crystallization under coulombic repulsion, a possibility mooted long ago in [1h]. This arrangement, though despite now satisfying the Yamada relation, does not meaningfully reflect the phase-slip behaviour of the spin array, and moreover it does not exhibit the necessary face-centring character within the *hole charge* array to match the x-ray diffraction results.

Note in figure 1 that the crystallographic basis to the *charge* face-centring geometry of the $8a_0$ supercell is the loose cluster of four holes about the stripe crossing-points. The orientation of this face-centring of the hole charge array is, we see, rotated by 45° as compared with the situation for the magnetic domains, and its forbidden spot positions are now the axial ones $\frac{1}{8}\mathbf{a}^*_0$ around the Γ points. Where evidence of diffraction spotting from the charge array is to

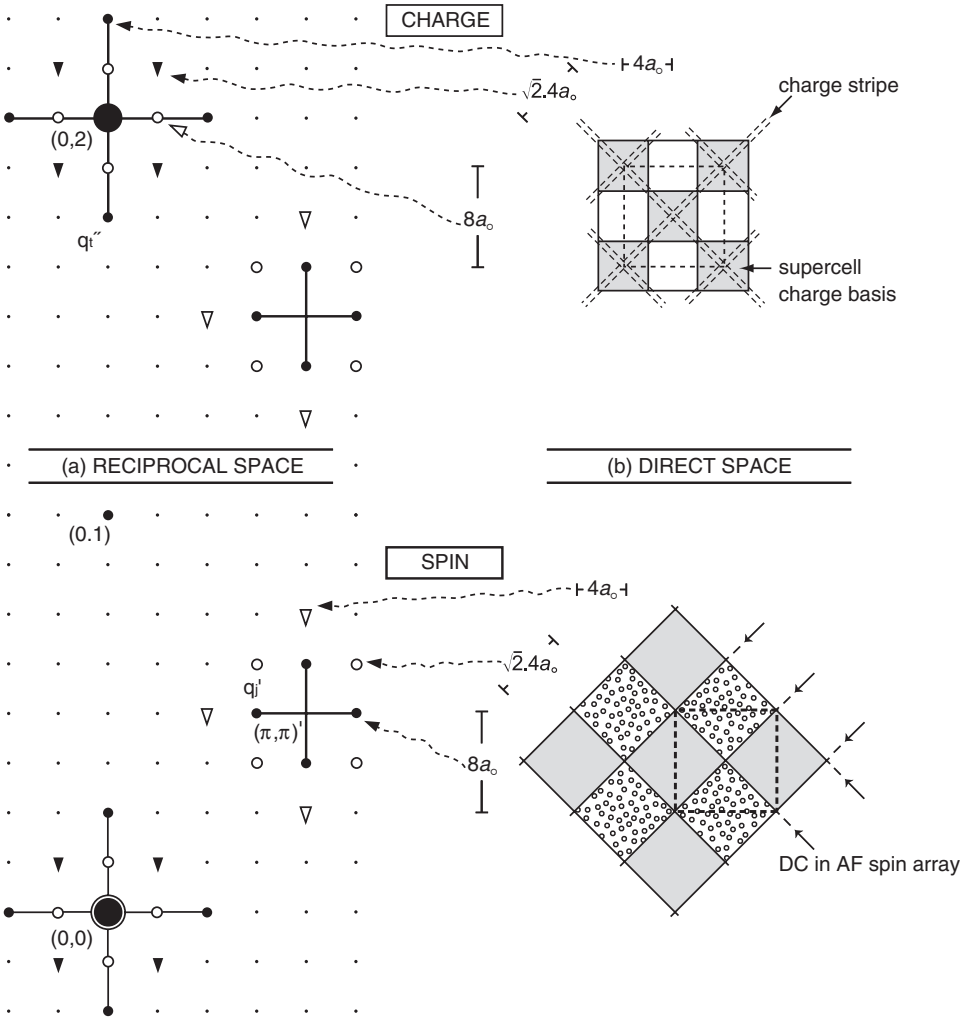

Figure 3. Real space and reciprocal space views of the 2-q charge and spin structures and resulting neutron diffraction, for the case of $p = \frac{1}{8}$ with its $8a_0$ square supercell. The charge stripe locations are indicated by the 45°-oriented, double-dashed lines, and the supercell's charge basis, containing four holes, is shown shaded. The $8a_0$ cell is face-centred with respect to this charge basis. The discommensurations (π-phase-slip boundaries) in the magnetic array superpose upon the charge stripes as indicated. The AF domains are 'up' and 'down' spin dominated (see figure 1), and they form two interpenetrating face-centred, 45°-rotated arrays, as indicated by the shading. The magnetic cell side is again $8a_0$. The charge array produces $\frac{2}{8}a_0^*$ (i.e. $\mathbf{q}_I''$) spotting and also diagonal spotting of wavevector length $\sqrt{2} \cdot \frac{1}{8}a_0^*$ (see [63]), with $\frac{1}{8}a_0^*$ itself forbidden. The magnetic array on the other hand produces $\frac{1}{8}a_0^*$ spotting (i.e. $\mathbf{q}_I'$), with this time $\sqrt{2} \cdot \frac{1}{8}a_0^*$ and $\frac{2}{8}a_0^*$ forbidden. The charge satellite spotting is to be centred around the Γ points for the bct crystal structure, $(m2, n2)a_0^*$, whilst the magnetic spotting devolves from the basic Néel structure spotting of the $p = 0$ Mott insulator sited diagonally at $(\frac{1}{2}, \frac{1}{2})a_0^*$, etc. Point (0, 1) is not equivalent to (0, 2) being a Z' point in bct geometry.

be gained, other than in the very weak $\frac{2}{8}\mathbf{a}_0^*$ spots—the $\mathbf{q}_I''$ of earlier—is in the diffuse x-ray scattering investigated by Issacs *et al* [63]. The latter develops in the diagonal directions as an x, y sum of the forbidden $\frac{1}{8}\mathbf{a}_0^*$ axial spots. Their work was in fact on a sample with a

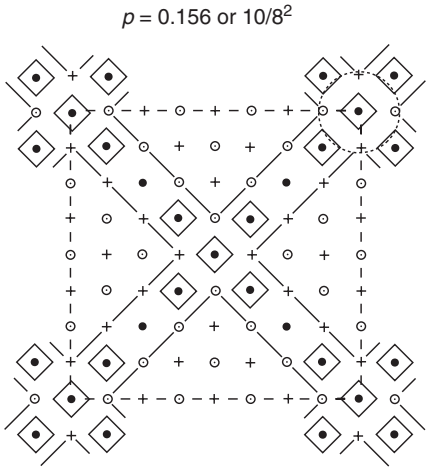

Figure 4. The proposed circumstance for where T_c becomes maximized. The structure is again an $8a_0$ cell as in figure 1, but now with two extra holes per cell occupying the stripe crossing points at the cell centre and corner. Of course this cell now is richer in holes than for the Yamada relation, having $p = 0.1562$ or $\frac{10}{8^2}$ in the $8a_0$ supercell. The five-hole clusters are seen as constituting very favourable pair production centres within the negative-U modelling adopted, the central site of the cluster being strongly Cu_{III}-like in nature. The large dotted circle running through the surrounding oxygen sites of the outer hole cells within the cluster is of diameter $\sqrt{5}a_0$. Calculations to be found in [67] would support this as marking the extended range of the interaction potential function to replace the $r = 0$ δ-function employed in the classic BCS treatment of superconductivity.

p value of only 0.075, and at this low and 'non-special' concentration the stripe organization automatically becomes less well perfected, the disorder greatly smearing the recorded diagonal diffraction.

Figure 3 provides a convenient summary now of the real space and reciprocal space situation encountered above, contrasting the diffraction behaviour arising from the spin and charge aspects to the striping.

4.2. $p = 0.1563$ or $\frac{10}{8^2}$ (figure 4). The optimization of T_c

This array sees the central site in the previous loose clusters of four holes now being occupied by a further hole. The hole number per cell thus grows by 2, but the cell size does not change, as evident in Niemöller *et al*'s x-ray work [59], from the early work of [64], and again more recently. Yamada *et al*'s results [53] showed that the simple $p\ (= n_h/A) = |\mathbf{q}_I'|$ relation becomes relinquished above $p = \frac{1}{8}$ to be replaced by a more complex progression of favoured arrangements.

From my own point of view the superstructure portrayed in figure 4 is highly favourable toward HTSC. It possesses five-centre clusters of holes into the heart of which the four axial Cu_{II} centres are able to afford low velocity x/y access for spin-opposed electrons. The Madelung potential at the central hole site has become strongly trivalent enabling it to act as electron pair production factory after the manner outlined above and throughout [1]. The fully embedded set of nine coordination units constitutes the appropriate cluster with which to endeavour to go forward now to a cluster dynamic mean-field theory evaluation [65] of the pairing process presented. It far supersedes in this regard the proposal rather hastily made in [66] for SNS2004, when first I started to consider the possibility.

I believe it not without theoretical intimation that the particular cluster pointed to above for future examination holds the form it does. The large dotted circle drawn in figure 4 through the outer oxygen atoms flanking the central coordination unit is of diameter $\sqrt{5}a_0$. Quintanilla and Gyorffy in [67] emerged with just such a pair interaction range (there numerically evaluated as $2.3a_0$) upon incorporating a cuprate band structure in their generalization of the BCS process to engage more closely the current mixed-valent, tight-binding situation. What that work sought was attempting to escape from the retarded, zero-range, pair interaction potential of the standard BCS approach, and to move to a finite-range, instantaneous interaction. The $\sqrt{5}a_0$ radius above would see the spin-opposed electron pair being received into the trivalent negative-U centre and installed largely over the oxygen sublattice. As was discussed earlier, this is where the accepting holes chiefly reside in the trivalent cuprates, unlike with the corresponding nickelates. The effect has the great benefit of relieving the very strong coulombic repulsion within a pair that would exist were the double occupancy fluctuation to be confined to the central Cu atom of the cluster.

A cluster of the above form does not have to owe its existence to stripe ordering, of course, it in large measure simply being an outcome of the given level of hole concentration, but striping will certainly increase its prevalence. It is important too to recall that at the present p value the striping does not terminate with T_c, but persists (at least in LSCO) to appreciably higher temperatures, as is to be seen in [64]. Clearly the striping is not the result of HTSC, but rather its facilitator. In our model, the negative-U pair production is going to add to the gapping of the axial fermionic saddle-point states under the diagonal bosonic pair scattering process [1c].

The value of p that currently we are focusing upon constitutes the doping level identified as being where in HTSC systems T_c universally is maximized. Note it in fact falls marginally below 0.16, the number to appear in the widely quoted empirical relation from [16] due to Tallon and co-workers, and extracted largely from transport data such as that to be seen in [32] and [35]. By $p = \frac{1}{6}$ one definitely has passed beyond the maximum in T_c. The neutron data of [30b] at that point reveal we have transferred to a new favoured supercell size, $\mathbf{q}'_1$ becoming $\frac{1}{7}\mathbf{a}^*_0$.

4.3. $p = 0.1837$ or $\frac{9}{7^2}$ (figure 5). The optimization of $n_s(p)$, $U_c(p)$ and $\chi(p)$

The new arrangement is gained upon reducing the above cell size from $8a_0$ to $7a_0$ by means of collapse of the previous loose cell-centring cluster to give a dense cluster of just four contiguous hole-bearing coordination units. The contracted cluster should be somewhat more amenable to treatment by CDMFT, and it still, note, displays the $\sqrt{5}a_0$ feature pointed to above. This new hole content is precisely that at which the specific heat work of [17] evaluates the condensation energy of the superconductivity (per hole) to have drawn up to its sharp maximum. Back where T_c maximized at $p = 0.156$, $U_c(p)$ was only a third of what it is to become by $p = 0.184$. The latter hole content additionally is where further analysis of the specific heat data would indicate the pseudogap, as extrapolated down from the normal state, to vanish. Effectively the same circumstance is in evidence in the recent Zn-doping work of [32a], the superconducting dome being found finally to collapse to zero at exactly this p value under steady advance in Zn concentration.

In all pure HTSC systems, $p = 0.184$ marks additionally, as long known, the doping level at which $\chi(T)$ becomes temperature invariant, separating a regime at low p where, due to residual spin coupling, $\chi(T)$ drops on cooling and a regime at higher p where $\chi(T)$ climbs on cooling. The latter condition is perceived to arise when the now decoupled spins are brought again to respond individually to the measuring field. As is to be seen from figure 5, it is geometrically possible within the present $p = \frac{9}{7^2}$ array to pair up all the domain spins there in RVB fashion. While the superconductive pairing force itself may already have peaked, pair

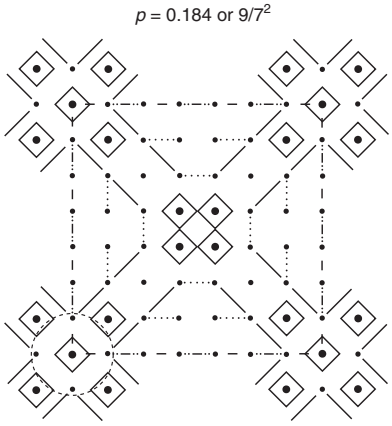

Figure 5. The situation proposed for the stage where the pseudogap vanishes and the superconducting condensation energy per pair, as deduced from the specific heat work [17], becomes maximized. It corresponds to $p = 0.1837$ or $\frac{9}{7^2}$. The $7a_0$ cell is reached from figure 4 by collapsing the central cluster from a loose five-hole one to a tight four-hole one. Again the large dotted circles are each of diameter $\sqrt{5}a_0$. The spins can here all be paired up in RVB fashion, appropriate to the fact that at this hole content most electrons become engaged in the superconductivity and the susceptibility is temperature independent with pair breaking low.

breaking becomes rendered here a minimum. Indeed, as the μSR 'boomerang' effect has earlier demonstrated [15], the total number of pairs at this point is brought to its maximum.

Finally it is here, too, that Komiya and co-workers have recently claimed they detect a slight anomaly in the normal state dc resistivity, comparable to the circumstance at $p = 0.125$, though considerably weaker [68]. The magic value that they suggest of $\frac{3}{16}$ or 0.1875, however, does not accord with their data quite so well as the figure which we here are pointing to of 0.1837.

The neutron work of Gilardi *et al* [58] using a LSCO sample having p in the current range of doping clearly supports our $7a_0$ ascription for the cell size. Often it has been asserted that all trace of such stripe phase organization rapidly becomes erased now if p is advanced any further towards 0.2. One suspects, however, that the circumstances might simply call for experimentation with x-rays instead of neutrons. Within the more ionic LBCO and LSCO families ordering phenomena certainly remain in evidence to well beyond $p = 0.2$.

4.4. $p = 0.250$ or $\frac{9}{6^2}$ and 0.277 or $\frac{10}{6^2}$ (figure 6). The relinquishing of HTSC

The recent neutron work on LSCO from Wakimoto *et al* [69] finds that by these values of p a $6a_0$ cell has become adopted. Figure 6 is drawn up for $p = \frac{1}{4}$ with the same general form as considered previously, but now contracted down to the $6a_0$ sizing and with no hole at the central site. Occupying the latter site by yet a further hole yields $p = 0.277$, the composition for which superconductivity finally is lost. By this stage the system has become so metallized that the potential, now densely packed, negative-U centres have been rendered ineffectual in pair production, the state energy having risen appreciably above E_F. The ionic Madelung potentials which locally had defined the binding, high valence, environment no longer are sufficiently unscreened to hold the state in the vicinity of E_F and allow the long duration, electron double-loading fluctuations.

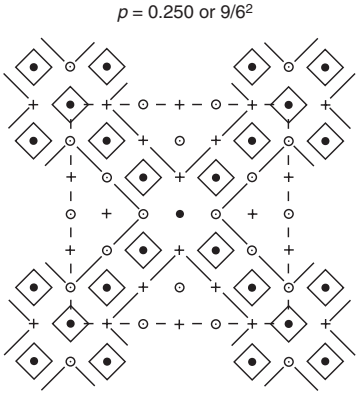

Figure 6. The dense array of charge stripes/magnetic discommensurations reached by $p = 0.25$. Adding a hole at the centre site of this $6a_0$ cell yields $p = \frac{10}{6^2}$ or 0.278, the point at which HTSC is terminated by the high level of metallization and a negative-U state that now lies above E_F.

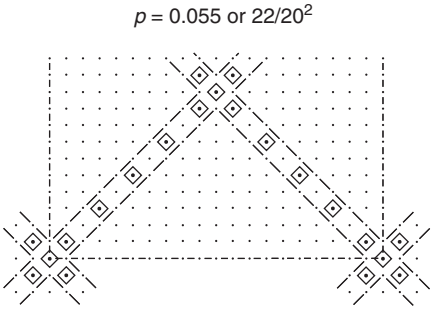

Figure 7. Half the $20a_0$ cell and stripe array corresponding to $p = \frac{22}{20^2}$ or 0.0550, below which composition the system passes over from axial 2-q to diagonal 1-q behaviour and HTSC finally is lost. The scale is half that of the previous figures. Removing one of the cluster-centring holes would give $p = 0.0525$ and removing both of course gives $p = 0.0500$, the Yamada composition. The level of organization of these dilute cases is probably increasingly difficult to sustain as the holes are required to be at rapidly growing separation from their corresponding substituent atoms.

4.5. $p = 0.055$ or $\frac{22}{20^2}$ (figure 7). The beginnings of HTSC and the 1-q–2-q choice

Above we had by $p = 0.278$ compacted down the preceding type of 2-q DC structuring as far as is meaningful. As was mentioned when assessing in section 3.3 the x-ray work of Ghazi *et al* [55] on the corresponding nickelates, this composition would support a 1-q faulting, terminating the progression of favoured structures identified there. Now at the other end of the composition scale, at the threshold to the spin-glass regime, there arises, similarly, clear evidence of 1-q striping becoming the favoured option. The work of Wakimoto and colleagues [70] performed on $(La_{2-x}Sr_x)CuO_4$ $x = 0.050$, as well as on 40% Nd-substituted material, clearly records at this point an asymmetry within the $\mathbf{q}'_I$ spotting. Instead of a cluster of four equal intensity spots, there occurs a $2 + 2$ break-up that clearly results from a uniaxial domain content in the now orthorhombic twinned samples. Furthermore in these circumstances the magnetic spotting transparently becomes associated with the diagonal 45° direction, under a domaining process involving just a single phase-slip direction. The phase-slip lines here adhere still to the 45° orientation, but now within a 1-q rather than a 2-q framework so that there no longer arises any face-centring of the array to complicate the diffraction outcome.

Upon increase in doping, as the DCs are brought closer together, quite suddenly one finds the diffraction pattern, for the LSCO system at least, to alter its character, as four-fold symmetry emerges in the magnetic spot intensities about π, π. With this change there arises the rotated x/y axial orientation of the $\mathbf{q}'_{\mathrm{I}}$. Likewise the *charge* spotting vectors about {2,0,0}, the $\mathbf{q}''_{\mathrm{I}}$, take on four-fold symmetry, as an inspection of figure 2(b) in the x-ray work from Issacs *et al* on LSCO $x = 0.075$ will show [63]. The low temperature condition is slightly orthorhombic still, but there now is no evidence of the observed pattern representing a multi-domain situation. One way to retain a single-q account of events could be for the 1D stripes to alternate in orientation within successive CuO_2 planes up the c-axis. However, there is no evidence of or reason for such c-axis order setting in sharply at 0.055. Indeed, owing to the rise in metallization, the drive to structural c-axis order should be weakening; Madelung forces would actually prefer to have the stripes AB-staggered, not crossed. Even when in the spin-glass regime the stripe ordering was not strongly coupled to the tilting corrugations of the LTO structure [70]. Circumstances could conceivably be somewhat different for the $YBCO_{7-x}$ system, where the chains provide stronger structural and electronic input, but, nonetheless, most diffraction data from YBCO remains remarkably four-fold symmetric in form.

The apparently terminal composition to support 2-q behaviour is $p = \frac{22}{20^2}$ or 0.055 and as represented in figure 7 it involves a $20a_0$ cell of 75 Å. A simple orthorhombic cell having $p = \frac{1}{20}$ would when still in the 1-q state call for a cell of size $\sqrt{2}a_0$ by $20a_0/\sqrt{2}$. The cell that Wakimoto *et al* present in figure 10 of [70] in order to yield a match with their diffraction data would appear not to be correct, it lacking, it seems, a factor of $\sqrt{2}$ to bring the assignment made there of 7 b_{ortho} up to 10 b_{ortho}.

For the situation given in figure 7, with its hole stripes in the 45° orientations, we may understand how quite good nodal conductivity is able to be retained so far towards the Mott insulating condition. Despite the quasiparticles being strongly drawn towards localization [71, 72], the conditions for pair coupling still are met with at the stripe crossing points, taking a vestige of HTSC behaviour right through to the spin-glass regime. The number of pairs however, inevitably will be small, because of the limited number of carriers and the now severe pair breaking from the spin array. It is noteworthy though that one finds from the outset $T_{\mathrm{c}}(p)$ to be a function displaying negative curvature remembering the positive curvature there for $n_{\mathrm{g}}(p)$ and $U_{\mathrm{c}}(p)$.

We are left at this point now to address two remaining important matters regarding the self-organization of spin and more especially charge in the mixed-valent HTSC cuprates.

(1) What is the source of the strong short-wavelength undispersed electronic modulations recently to have been uncovered by energy-resolved STM work as one approaches localization, this irrespective of whether through reducing p (locally or globally), or raising T, or under an applied magnetic field?
(2) Is charge striping truly origin to the incommensurate magnetic response at $\mathbf{q}'_{\mathrm{I}}(\omega, T)$ witnessed experimentally?

5. Checker boards and spin waves: what is their reality?

5.1. Checkerboard behaviour as competition at the saddles regarding superconductive pairing

We now should look at what the form and origin are of the non-dispersive, short wavelength, electronic modulations recently to have been detected in a wide range of STM probings of HTSC systems as these are taken towards Mott–Anderson localization. This may be accomplished in a global way via the level of underdoping, or one can shift to a system that is more ionic by some appropriate selection of the counter-ions, both cations and anions. One alternatively can with STM specifically elect to examine those nanoregions which by

virtue of the statistical nature of the doping happen to stand closer to localization. The tunnelling spectrum indicates clearly where and whenever the probe falls within a nanoregion locally supporting superconductivity or has passed into one in which the pseudogap regime holds. It is possible, alternatively again, to examine the pseudogap regime within otherwise superconducting material upon the application of a magnetic field, and then look in the vicinity of a current vortex created around a quantized flux-line. A yet further way to reach the pseudogap regime is to warm the sample up a little above T_c. The latter is a difficult route for STM experimentation, but it has been successfully pursued by Vershinin and colleagues [73]. The magnetic field route was pioneered by Renner *et al* [74], and more recently has been taken up by Hoffman *et al* [75] The underdoping route has been explored by Davis and colleagues as well [76, 77], and their work has much increased the attention paid to the strongly modulated 'checkerboard' spatial images recorded once outside the superconducting nanoregions. Where such images now have become pre-eminent is in Hanaguri *et al*'s recent work [78] on $(Na_xCa_{2-x})CuO_2Cl_2$ [Na-CCOC]. The latter is one of the most ionic of HTSC systems yet investigated and it provides remarkably sharp modulation images. These persist to high tunnelling voltages (up to 100 mV), whether employing a sample bias that is positive (electron injection) or negative (stronger signal; electron extraction $\equiv$ hole injection). Why so much interest exists in the pseudogap condition is that towards the Mott regime the state is perceived as vying with the occurrence of HTSC, in particular as concerns the way it relates to the Fermi surface hot-spot regions, so important to superconductive pairing whether by spin fluctuations [79] or in our negative-U scenario [1].

The dispersionless periodicities detected in the various STM experiments referred to above cover a fair range from just below $4a_0$ to up towards $5a_0$, $4a_0$ frequently being quoted. Because of that, the phenomenon has become known loosely as '$4a_0$ checkerboarding'. Unfortunately this usage has spawned a large and exotic series of real space based suggestions as to its origin [80–87]. However, the restricted periodicity range being reported would suggest here some k-space related effect. Certainly the effect is electronic in nature rather than atomic (as might just possibly have arisen from, say, some more complex Jahn–Teller arrangement) with no trace left in standard x-ray or neutron crystallography. Two very pertinent observations are that the more underdoped a sample is the shorter becomes the primary modulation wavelength reported, and the more ionic the system becomes the sharper its definition. In the Na-CCOC case [78] and for samples to either side of the threshold to a delayed superconductivity around $p = 0.07$, the effect has become there so strong and the images (obtained at 10 mK and positive sample bias) so complex that they readily support a full Fourier analysis of what is occurring. Such analysis shows that the images predominantly emerge here from an admixture of k-values of $\frac{1}{4}\mathbf{a}_0^*$, its complement $\frac{3}{4}\mathbf{a}_0^*$, plus $\mathbf{a}_0^*$ directly [78]. The shortest of these k-vectors could suggest the separation between quasiparticle states across the individual arms of the Fermi surface near the saddle points—exactly the hot-spot regions. However, at first sight there exists a considerable bar to such an ascription—namely the k-space span across the arms is from LDA band structure calculations [88–90] not this large, in ordinary circumstances. A simple construction based on a circular Fermi surface centred upon the zone corner would at $p = 0.12$ yield an arm spanning vector of only $\frac{1}{6.4}\mathbf{a}_0^*$, not $\frac{1}{4}\mathbf{a}_0^*$. Recent experimental detailing by ARPES [91] and STM [8, 1a] of the Fermi surface geometry appears, however, to assert that the real situation is otherwise, and would afford relief to such an impasse. How can this be?

Some years ago photoemission results indicated that the saddle point regions of the band structure were disproportionately renormalized by correlations, consequent upon their x/y axial position, their low binding energy, and the $d_{x^2-y^2}$ σ^* wavefunctions specifically involved. The early ARPES work of Gofron *et al* [92], of King *et al* [93], and of Ma *et al* [94], conducted on both optimally and somewhat underdoped material, all in fact reported that, as compared

with LDA calculations, the saddle features appear much elongated along the x- and y-axes, and in such material would seem to be pinned some 20 meV or so below E_F. Moreover more recent ARPES data, of now greatly improved resolution and having the ability to separate the bonding and antibonding components arising from the bilayer interaction in BSCCO, have encouraged the notion of a progressive 'unzippering' of the Fermi surface back from the antinodes towards the nodes, as the level of hole doping is diminished [11, 95]. That a strong scattering- and correlation-driven gapping steadily is being introduced into normal state behaviour first was in evidence in the rising Hall coefficient found upon cooling, and in the marked effect the ionicity of the counter-ions is able to play here [1f, 96, 97], an effect reversed by the application of hydrostatic pressure [98]. A result echoing the Hall behaviour is the driving up of the Seebeck coefficient upon cooling [10]. The latter effect is, of course, the one lying behind the commonly employed method to assess doping content introduced by Obertelli *et al* [99].

Precisely how correlations and the approach to the Mott transition initiate pseudogapping and ultimately elimination of the Fermi surface, beginning with the antinodes and working back towards the nodes, has become a matter of considerable theoretical endeavour. Khodel and co-workers [100] were the first in their 'fermion condensation' work to indicate just how the specific band structure of the HTSC cuprates lends itself to appreciable renormalization under the action of strong correlations. The renormalization takes the form not only of a pinning of the energy of the Van Hove singularity, but also the straightening out of the Fermi surface geometry at the saddles along with increase in the lateral extent in k-space of the states occupied there. This same type of deformation of the Fermi surface geometry at the saddles has been arrived at too now through the very different approach of cluster DMFT by Civelli *et al* [101], and again by Carter and Schofield [102]. An expanded Fermi sea around the hot spots and its pathologically straightened form (we shall use the term 'boxing') are precisely what we were seeking in order to account for the observed checkerboarding activity.

Note that the checkerboard signal in the STM work is marked by a diminished conductance, not enhanced conduction as would come from a classical charge density wave. The injected electrons (abstracted holes) are non-propagating for the set spanning wavevector. Not only is this the case with the $\frac{1}{4}\mathbf{a}_0^*$ modulation, but also for its complement, the $\frac{3}{4}\mathbf{a}_0^*$ wave [78]. The relative degree of 'boxing' and 'unzippering' of the Fermi surface across the progression BSCCO, LSCO and Na-CCOC of HTSC cuprates of steadily increased ionicity is most striking [103, 104]. A higher ionicity for the cationic counter-ions forces the upper oxygen-based valence band states to greater binding energies and thereby reduces the p/d mixing within the CuO_2 planes. This means that the correlation effects become more marked then at any particular hole doping. Conversely, under increased covalency the saddle is free to drop away from E_F with increased underdoping at somewhat greater p values and at less departure from the M point. The binding energy associated with the saddles is largely what tunnelling and ARPES here register, and as with the 'large pseudogap', this energy can amount to one or two tenths of an eV in strongly underdoped material. The above features dovetail almost by accident onto the superconducting gap for samples near optimal doping. As regards the *small energy* pseudo-gapping (principally coming from spin), active throughout in the vicinity of E_F, this ultimately opens up into an actual gap in LSCO for p below 0.055. And as one approaches this latter juncture what has become of the lateral extent of the saddle arm? It is $\approx 0.25\mathbf{a}_0^*$ [103] (see figure 8 to be discussed in detail below).

As was observed in the above recent comparative ARPES study from Tanaka *et al* [103], as well as in earlier analysis by Tohyama and Maekawa [105] of Ino *et al*'s LSCO ARPES work [106], what correlation particularly influences within the band structure is the relative magnitude of t', the second-nearest-neighbour (diagonal) hopping parameter. The latter, for the given wavefunctions and crystal structure, bears reversed sign within the tight-binding

Hamiltonian to t and t''. The t' integral is governed primarily by overlap over the oxygen sublattice, and so becomes particularly sensitive to the degree of covalence in these systems.

The doping-dependent evolution of events reported in Ino *et al*'s ARPES work on LSCO [106] repays close attention now. The way in which the Fermi surface modifies its conformation in figure 7 there from $x = 0.30$ to 0.05 is most revealing. The construction of that figure presumed that the Luttinger sum rule remains satisfied throughout. This assumption necessarily has to be embraced because for LSCO the experimental definition of E_F in the spectra below $x = 0.12$ becomes very poor in the nodal directions. Recall that even the nodal directions suffer significant scattering and do not afford 'good metal' behaviour [1c, 9, 107]. The sharper definition of the spectral onset found in the vicinity of the antinodes arises in large measure not from any well-defined metallic behaviour there, but rather from the strongly constrained DOS, with its incipient Mott gapping above T_c, supplanted in part by the superconductive gapping once below T_c. Within the negative-U modelling of the B–F scenario, the local pairs precipitate Cooper pairing amongst the quasiparticles far around the Fermi surface in feed-back fashion.

Remember from the μSR work that once in the superconducting state one finds n_s comes to its peak near $p = 0.185$ [15]. Upon reduction in 'hole content' p, a smaller and smaller fraction of the quasiparticles from what was the Fermi surface become able to be drawn into the *superconductive* condensate, causing the condensate energy per gram-atom (assessed near and below T_c) to drop away rapidly. According to the specific heat results of Loram *et al* [17], $U_c(0, p)$ declines from its peak value at $p = p_c = 0.184$ very steeply, and indeed for the case of Bi-2212 the results of figure 8 in [17b] plot out as being exponential in form. Matsuzaki *et al* [108] recently have presented their LSCO specific heat results as supporting the functional form of $U_c(0, p)$ to be only quadratic. They decompose this then as $\propto p \cdot \Delta(p)$, where in turn $\Delta(p) = p \cdot \Delta^o(p = 0.183)$. Within my own negative-U interpretation the higher power of p^4 might at first sight appear more viable, an initial factor here of p^2 reflecting the growth in concentration of the negative-U centres, with the second factor of p^2 representing the effective reaction rate for electron–electron pairing collisions at those centres, under the tripartite negative-U process. However, a variation faster than power law form has to be anticipated when we factor in the added effect of the pseudogapping and of its rapid termination towards p_c. This extra factor mounts rapidly with p from being zero at $p = 0$ to unity near $p = 0.184$. Approaching the latter composition the pseudogap magnitude has for most $\mathbf{k}_F$ become rendered smaller than the corresponding superconducting gap.

The scale constructions that I append in figures 8 should help to clarify the above-discussed changes which correlation is imposing upon the effective Fermi surface character and geometry as the hole doping level is altered. Note that in their LSCO ARPES work Ino *et al* [106] at $x = 0.15$ assessed the nodal crossing point to be $\sim 0.40(\pi, \pi)$. Such a value declares immediately that the heavily correlated surface displays reverse curvature to what for a very considerable time was believed to hold for LSCO at optimal doping. The 'boxing up and unzippering' of the Fermi surface saddles being spoken of above would, if extended in the same manner right through to the Mott insulator at $p = 0$, carry the nodal point there back to $\sim 0.30(\pi, \pi)$ and see the corresponding arm spanning vector raised to $\mathbf{a}_0^*/3.4$. At the other limit of $p = 0.184$, upon employing a near-circular Fermi surface centred at the zone corner, one emerges with an arm spanning vector reduced to $\sim \mathbf{a}_0^*/7.5$. By the latter stage the checkerboarding should have evaporated, and the entire Fermi surface action be incorporated now into the superconductivity. Note that the above-outlined pseudogap behaviour is the very antithesis of the Fermi surface nesting behaviour of a more customary circumstance, and it appropriately is associated with a minimum in the STM conductance measured between atom sites related by the dilated saddle spanning wavevectors.

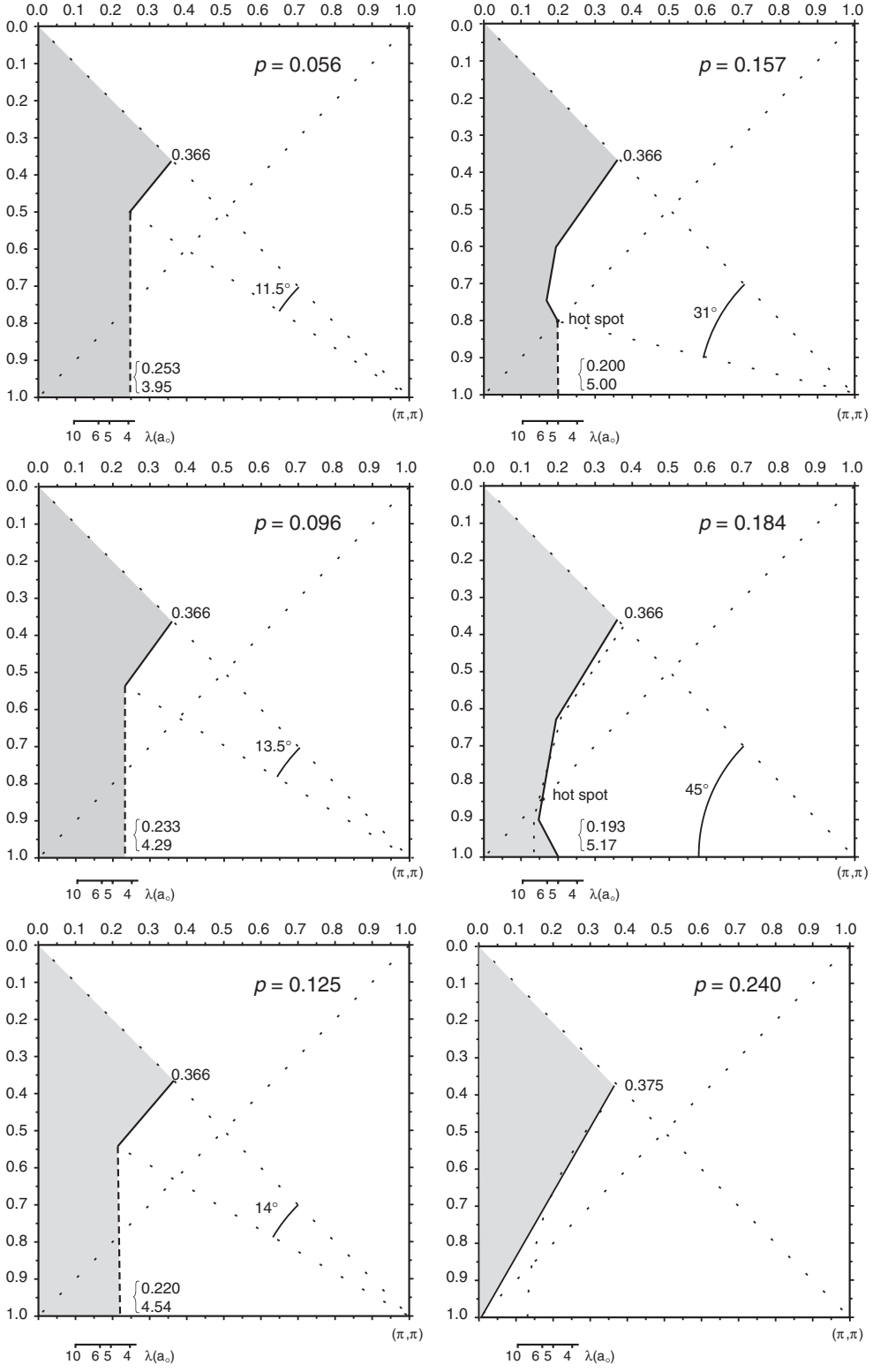
p = 0.056
0.366
11.5°
0.253
3.95
p = 0.157
0.366
hot spot
31°
0.200
5.00
p = 0.096
0.366
13.5°
0.233
4.29
p = 0.184
0.366
hot spot
45°
0.193
5.17
p = 0.125
0.366
14°
0.220
4.54
p = 0.240
0.375
0.0 0.1 0.2 0.3 0.4 0.5 0.6 0.7 0.8 0.9 1.0
(π,π)
10 6 5 4 λ(a∘)

Figure 8. Scale constructions of the Fermi surface in the repeat octant of the zone at the hole doping levels $p = 0.056$, 0.096, 0.125, 0.157, 0.184 and 0.240. Where the surface is strongly pseudogapped in the saddle region below $p = 0.184$ that segment is indicated by a dashed line. A solid line is used nearer the nodal direction where the carriers are freer. The nodal intersection point is based on ARPES results, whilst the 'boxed' saddle region follows the interpretation given in the text of the STM checkerboarding results. The occupied and unoccupied areas of the zone are accurately in compliance with Luttinger's theorem. The large dotted circle appearing in the $p = 0.184$ and 0.240 plots is the Fermi surface appropriate to free electrons at $p = 0.200$. The boxed segment spanning modulation wavelength covers the range from range from 4 to 5 a_0 seen in the STM work. The curves have been left unsmoothed to permit understanding of what is presented and register clearly the evolution of form.

Having introduced the general line of argument, it now is time to examine some of the emergent detail more closely. Figures 8(a)–(f) have been constructed in line with the information deriving from the observed checkerboarding wavevectors, treated as above, and also the ARPES results of Ino *et al* for LSCO already referred to [106]. When the ARPES results are examined really closely it becomes very evident that extracting hard numbers for the precise location of the Fermi level intersection wavevectors is highly problematic, even in these 11 K spectra. Indeed because, for most of the compositions studied, 11 K puts us in the $d_{x^2-y^2}$ superconducting regime, and with the pseudogapping well advanced, such a temperature of operation introduces its own problems. Always, besides, a substantial background needs to be removed that is not structureless in the vicinity of E_F. As Ino *et al* state, the particularly poor definition of the spectral onset found in the nodal direction for $p < 0.125$ means, too, that Luttinger's theorem has routinely to be invoked. Fortunately there occurs relatively very little movement of the nodal intersection point with p, and throughout figure 8 (apart from the case of $p = 0.24$) I have chosen to hold its location constant at 0.366 (π, π). The ARPES spectrum labelled 0.37 actually was highlighted in figure 2(c) of [106] for $p = 0.15$, but it was the neighbouring curves identifying 0.41 that were picked out both in figures 1(c) and 3(c) of [106] for the flanking compositions $p = 0.22$ and 0.05, whereas I would prefer to stick with the lower value. Figure 7 in [106] indeed becomes in effect a general schematic rather than a close rendering of the detailed evolution of the Fermi surface shape. Some of the identifications offered of the intersection points in the present key 0, π to $-\pi, \pi$ saddle spanning directions are very dubious indeed, even after following the double differentiation technique suggested. As to my own offerings in figure 8 regarding Fermi surface evolution, I have throughout these geometrical constructions again adhered to Luttinger's theorem. The pseudogapping is perceived as transferring ARPES spectral weight to higher binding, but leaving the k-space representation for the 'diluted' coherent residue in place—simply holding reduced weighting. I have chosen not to smooth out the evaluated boundary lines separating occupied and unoccupied k states in order to permit the proposed evolution of the demarcation line to be plainly evident. Where the Fermi level effectively is gapped over the boxed 'vertical' stretches has been marked with a broken line, whilst a solid line is used where the behaviour is deemed more standard. From the figures one observes how up to $p \sim 0.125$ the Fermi arc spreads out rather slowly from the nodal point, whilst between $p = 0.125$ and 0.184 the 'freed' section expands very rapidly, as the 'boxed' segment shrinks back towards the zone-face saddle point. This process reflects what was disclosed in the specific heat data regarding the run-away growth in $U_c(0, p)$, as discussed above [17, 108].

The sixth curve in the set is constructed for $p = 0.24$, and it marks the point where the Fermi surface just necks off at the saddle. This is where the Hall coefficient goes negative [109]. It does not, however, quite see the end of strongly correlated behaviour. As is well known the magnetic susceptibility actually is in the process of experiencing increased temperature dependence [110], whilst the resistivity still remains sizeable and, most significantly, bears

a purely T^2 temperature dependence to more than 50 K [111]. Then, of course, the HTSC behaviour extends a little further yet.

5.2. Stripes versus spin waves: the matter of dispersion

The persistence of strong correlation right over the superconducting range encourages those looking towards a spin fluctuation interpretation of HTSC to persist with an RPA type treatment of the generalized susceptibility $\chi(\mathbf{q}, \omega)$, appropriate to a somewhat more standard metal like chromium or VSe_2, down into the more localized regime where HTSC flourishes. I cannot believe this is a legitimate extension, and indeed, as normally conducted [79], it would place no low-p bound upon the rise of T_c. Furthermore, in order to gain a match with experiment, it calls for the employment of a p-independent Hubbard U value of only $\approx$1 eV, and that at a time when the correlation is rising sharply towards the Mott insulating condition. In my own negative-U scenario, the optical and laser pump–probe results [1d] would indicate the negative-U σ^* collapse exactly to off-set a positive U value of 3 eV (per pair) so creating a local pair energy resonance with the quasiparticles. These latter values for the HTSC cuprates are suited to being in the BCS/BE crossover regime, where $|U|$ is $\sim$ the bandwidth W, and it is at just this stage that T_c becomes maximized [112].

The spin fluctuation approach perceives the charge and lattice response [79] as being subsidiary in HTSC matters, whereas the negative-U route regards the magnetic response to be the secondary aspect. As was stated previously, the former view has come about because of the dominant position of the neutron scattering results within the hierarchy of HTSC phenomenology. The reluctance to embrace the central role of dynamic charge striping as being behind the incommensurate spin scattering of neutrons has been truly remarkable [113, 114], and has not been dispelled by the synchrotron radiation mirroring of events [59]. This unfortunate situation has revolved around the interpretation of what the so-called 'magnetic resonance peak' to be seen in the vicinity of 40 meV for HTSC systems with $T_c(p)^{max} \sim 90$ K really represents. In my own reading the latter simply is a monitor of spin-flip pair triplet excitation, and as such accounts for its energy relation to T_c being around $5\frac{1}{2}\ k_B T_c$, appropriate to strong coupling d-wave superconducting behaviour. This spin-flip energy is slightly smaller than the longitudinal plasma resonance energy of the condensate sensed by electron energy loss spectroscopy [1a, 115] and to which the extra band 'kinking' found near the saddle point of the band structure [116] may be attributed [1a]. All three features are directly related to the carrier pairing, and all evaporate in the environs of T_c. The stripes, on the other hand, like the somewhat higher energy kinking to be observed in the *nodal* band dispersion, run through to higher temperatures [9, 113] as befits charge/lattice effects not primarily linked to the superconductivity itself. As mentioned earlier such charge effects relate through to the similar behaviour obtained with the non-superconducting cuprates for $p < 0.055$ [70] and to the nickelates [55]. Indeed, as we have seen, the charge stripes and the associated magnetic discommensurations acquire spacing periodicities in the cuprates that are not related to fermiology but to dopant numerology. Even where events do appear to become dictated by the Fermi surface geometry in the STM-registered checkerboarding [77, 78] discussed above, we patently are in a regime for which standard metal physics must be inapplicable.

What then are we to make of the claim that the incommensurate neutron diffraction wavevector is energy dependent, and resembling what at first sight one might expect of antiferromagnetic spin-wave dispersion, albeit now in an incommensurate setting as if governed by Fermi surface nesting (see [113]). One firstly must recall this spin scattering is generated only in the limited energy range where composition and temperature put one above the spin-gap state being settled into at lower temperatures and energies. Now were the magnetic discommensuration periodicities simply to follow those of the charge self-organization stripes,

as developed in section 3.4, ought one not to expect the wavevectors in question to display very little energy dependence?—certainly not to the degree suggested by figure 4 in [113]. What I would propose actually is being encountered in [113] ensues from two distinct sources. First, the resonant peak, as spin-flip excitation, has a dispersion from π, π that is downwards toward lower binding energies, reflecting the $d_{x^2-y^2}$ origins to the quasiparticle pairing [1a, 117]. Note that in LSCO $5\frac{1}{2}k_B T_c^{max}$ is only 17 meV, and with this more ionic single layer system a much less sharply defined feature is formed than in YBCO and BSCCO. Second, whether via thermal or direct excitation, the charge stripe organization suffers in conjunction with the quasiparticle self-energy to the extent that many carriers lose quantum coherence. The result is a transfer of much weight from the sharp IC spotting of the charge/spin organized state back into diffuse short-range AF interaction about π, π. It is my impression that much of the apparent modal dispersion arises from such causes, together with the added potential for some actual localization of the hole carriers diminishing the contribution to the active hole number count that determines the IC striping wavevector and thereby causing the latter to shrink back on π, π. At the very least it would be good at this point to see a five-peak analysis of the neutron diffraction data replace the customary four-peak analysis (even as adjusted by an inverse correlation function $\kappa(\omega)$). The fact that the striping geometries detected dovetail smoothly onto those of the d^7/d^8 nickelates, and indeed onto the cuprates in the Mott insulating condition below $p = 0.055$, surely implies that the fermiology hand is being overplayed in this matter. Our above-proposed understanding of the checkerboarding phenomenology would much endorse this conclusion.

6. Conclusions

An attempt has been made to show how a further detailed body of experimental results can be presented within the framework of the negative-U boson–fermion modelling of HTSC cuprates developed previously in [1]. We have concentrated here on various lattice-based phenomena, revealing how these create the detailed conditions within which the unusual electronic behaviour proceeds. The strong lattice responses arise due to proximity to the Mott transition and because in the cuprates we are dealing with σ/σ^* rather than π/π^* orbitals. This makes Jahn–Teller effects much stronger, securing charge segregation and striping via strain and Coulombic means rather than by Fermi surface nesting. Where something akin to Fermi surface spanning physics does arise appears to be in the checkerboard generation which emerges under the action of pseudogapping, and as such it is actually then outside the range of normal metal physics. The hole charge striping is seen to entrain a magnetic discommensuration array within the antiferromagnetic order between the interchain domains. The charge and spin arrays are in most circumstances in fact 2-q in form and not 1-q, and each is associated with face-centred geometry. This latter feature accounts for the observed well-known patterns of diffraction spotting, both charge and spin. The arrays are in general formed only dynamically, being primarily associated with the excess dopant charge rather than the frozen dopant ions themselves. However, relatively long-lived, highly local environments are established from both sources. It would appear that the presence of such strong and relatively unscreened nanostructure lies at the heart of the creation of local pairs which drives forward superconductivity under the boson–fermion resonance attained by virtue of the negative-U state inversion. Two cluster geometries have been identified with which to try to advance to a numerical evaluation of the proposed HTSC mechanism, employing the cluster dynamic mean field theory techniques currently under development. The clusters suggested are in line with the preliminary results from CPA treatments of the pairing, obtained by working from standard LDA band structures. They are the ones favoured by diagonal 2-q striping.

Acknowledgment

The author would like to thank the Leverhulme Trust for their financial assistance in making the continuation of this work possible.

References

[1a] Wilson J A 2004 *Phil. Mag.* **84** 2183
[1b] Wilson J A 2001 *J. Phys.: Condens. Matter* **13** R945–77
[1c] Wilson J A 2000 *J. Phys.: Condens. Matter* **12** R517–47
[1d] Wilson J A 2000 *J. Phys.: Condens. Matter* **12** 303–10
[1e] Wilson J A 1998 *J. Phys.: Condens. Matter* **10** 3387–410
[1f] Wilson J A and Zahrir A 1997 *Rep. Prog. Phys.* **60** 941–1024
[1g] Wilson J A 1994 *Physica* C **233** 332–48
[1h] Wilson J A 1989 *Int. J. Mod. Phys.* B **3** 691–710
[1i] Wilson J A 1988 *J. Phys. C: Solid State Phys.* **21** 2067–102
Wilson J A 1987 *J. Phys. C: Solid State Phys.* **20** L911–6
[2] Röhler J 2004 *J. Supercond.* **17** 159
[3] Altman E and Auerbach A 2002 *Phys. Rev.* B **65** 104508
Lee P A, Nagaosa N and Wen X-G 2006 *Rev. Mod. Phys.* **78** 17
[4] Marsiglio F, Teshima R and Hirsch J E 2003 *Phys. Rev.* B **68** 224507
but also see Hirsch J E 2004 *Preprint* cond-mat/0407642
[5] Alexandrov A S 2004 *Preprint* cond-mat/0408622
[6] Singer P M, Hunt A W, Cederström A F and Imai T 2003 *Preprint* cond-mat/0302077
Singer P M, Hunt A W and Imai T 2003 *Preprint* cond-mat/0302078
[7] Savici A T *et al* 2002 *Phys. Rev.* B **66** 014524
[8] McElroy K, Lee D-H, Hoffman J E, Lang K M, Hudson E W, Eisaki H, Lee J and Davis J C 2004 *Preprint* cond-mat/0404005
[9] Koitzsch A, Borisenko S V, Kordyuk A, Kim T K, Knupfer M, Fink J, Berger H and Follath R 2004 *Phys. Rev.* B **69** 140507
[10] Wilson J A and Farbod M 2000 *Supercond. Sci. Technol.* **13** 307
[11] Zhou Y J *et al* 2004 *Preprint* cond-mat/0403181
Yoshida T *et al* 2003 *Phys. Rev. Lett.* **91** 027001
[12] Wang Y, Ono S, Onose Y, Gu G, Ando Y, Tokura Y, Uchida S and Ong N P 2003 *Science* **299** 86
[13] Uemura Y J *et al* 1989 *Phys. Rev. Lett.* **62** 2317
[14] Zuev Y, Kim M S and Lemberger T R 2004 *Preprint* cond-mat/0410135
[15] Uemura Y J 1997 *Physica* C **282–287** 194
Uemura Y J 2000 *Int. J. Mod. Phys.* B **14** 3703 (*Preprint* cond-mat/0406301)
[16] Presland M R, Tallon J L, Buckley R G, Liu R S and Flower N E 1991 *Physica* C **176** 95
Tallon J L and Flower N E 1993 *Physica* C **204** 237
[17a] Loram J W, Mirza K A and Cooper J R 1998 *Research Review 1998 HTSC* ed W Y Liang (Cambridge: University Press) pp 77–97
Loram J W, Luo J, Cooper J R, Liang W Y and Tallon T L 2000 *Physica* C **341–8** 831
[17b] Loram J W, Luo J, Cooper J R, Liang W Y and Tallon T L 2001 *J. Phys. Chem. Solids* **62** 59
[18] Domanski T and Ranninger J 2001 *Phys. Rev.* B **63** 134505
Domanski T and Ranninger J 2003 *Phys. Rev. Lett.* **91** 255301
Domanski T and Ranninger J 2004 *Preprint* cond-mat/0409359
Domanski T 2003 *Phys. Rev.* A **68** 013603
[19] de Llano M 2004 *Preprint* cond-mat/0405071
Aguiler-Navarro V C, Fortes M and de Llano M 2004 *Solid State Commun.* **129** 577
[20] Alexandrov A S 2004 *Phil. Mag.* **84** 3299
[21] Birgeneau R J *et al* 1988 *Phys. Rev.* B **38** 6614
[22] Antipov E V, Abakumov A M and Putilin S N 2002 *Supercond. Sci. Technol.* **15** R31
[23] Sonier J E *et al* 2001 *Science* **292** 1692
[24] Anderson P W 2004 *Preprint* cond-mat/0406038
[25] Lake B, Aeppli G, Mason T E, Schröder A, McMorrow D F, Lefmann K, Isshiki M, Nohara M, Takagi H and Hayden S M 1999 *Nature* **400** 43

[26] Reznik D, Bourges P, Pintschovius L, Endoh Y, Sidis Y, Masui T and Tajima S 2004 *Phys. Rev. Lett.* **93** 207003

[27] He H, Bourges P, Sidis Y, Ulrich C, Regnault L P, Pailhès S, Bergigiarova N S, Kolesnikov N N and Keimer B 2002 *Science* **295** 1045

[28] He H *et al* 2001 *Phys. Rev. Lett.* **86** 1610

[29] Kudo K, Yamazaki M, Kawamata T, Adachi T, Noji T, Koike Y, Nishizaki T and Kobayashi N 2004 *Phys. Rev.* B **70** 014503

Savici A T *et al* 2004 *Preprint* cond-mat/0410652

[30a] Lake B *et al* 2002 *Nature* **415** 299

[30b] Lake B, Aeppli G, Clausen K N, McMorrow D F, Lefmann K, Mangkorntong N, Nohara M, Takagi H, Mason T E and Schröder A 2001 *Science* **291** 1759

[30c] Lake B *et al* 2005 *Nature Mater.* **4** 658

[31] Nachumi B *et al* 1996 *Phys. Rev. Lett.* **77** 5421

[32a] Naqib S H, Cooper J R, Islam R S and Tallon J L 2004 *Preprint* cond-mat/0408203

[32b] Nakano T, Monomo N, Matsuzaki T, Nagata T, Yokoyama M, Oda M and Ido M 1999 *Physica* C **317/8** 575

[33] Kofu M, Kimura H and Hirota K 2004 *Preprint* cond-mat/0409747

[34] Tallon J L, Bernhard C, Binninger U, Hofer A, Williams G V M, Ansaldo E J, Budnik J I and Niedermayer C 1995 *Phys. Rev. Lett.* **74** 1008

[35] Tallon J L, Bernhard C and Shaked H 1995 *Phys. Rev.* B **51** 12911

[36] Bernhard C, Niedermayer C, Binninger U, Hofer A, Tallon J L, Williams G V M, Ansaldo E J and Budnick J I 1994 *Physica* C **226** 250

[37] Edwards H L, Barr A L, Markert J T and de Lozanne A L 1994 *Phys. Rev. Lett.* **73** 1154

[38] Islam Z *et al* 2004 *Phys. Rev. Lett.* **93** 157008

Strempfer J, Zegkinoglou I, Rütt U, Zimmermann M v, Bernhard C, Lin C T, Wolf T and Keimer B 2004 *Phys. Rev. Lett.* **93** 157007

[39] Massidda S, Yu T, Freeman A J and Koelling D D 1987 *Phys. Lett.* A **122** 198

Massidda S, Yu T, Freeman A J and Koelling D D 1987 *Phys. Lett.* A **122** 203

[40] Wilson J A 1972 *Adv. Phys.* **21** 143

[41] Haase J, Sushkov O P, Horsch P and Williams G V M 2004 *Phys. Rev.* B **69** 094504

[42] Yvon K, Bezinge A, Tissot P and Fischer P 1999 *J. Solid State Chem.* **65** 225

[43] Winkler B, Pickard C J, Segall M D and Milman V 2001 *Phys. Rev.* B **63** 214103

[44] Haskel D, Stern E A, Hinks D G, Mitchell A W and Jorgensen J D 1997 *Phys. Rev.* B **56** R521

[45] Dmowski W, McQueeney R J, Egami T, Feng Y P, Sinha S K, Hinatsu T and Uchida S 1995 *Phys. Rev.* B **52** 6829

Billinge S J L and Duxbury P M 2002 *Int. J. Mod. Phys.* B **16** 1697

[46] Saini N L, Oyanagi H and Bianconi A 2004 *J. Supercond.* **17** 103

[47] Farbod M, Giblin S, Bennett M and Wilson J A 2000 *J. Phys.: Condens. Matter* **12** 2043

[48] Tranquada J M, Sternieb B J, Axe J D, Nakamura Y and Uchida S 1995 *Nature* **375** 561

[49] Fujita M, Goka H, Yamada K, Tranquada J M and Regnault L P 2004 *Phys. Rev.* B **70** 104517

(See also Kimura H, Noda Y, Goka H, Fujita M, Yamada K, Mizumaki M, Ikeda N and Ohsumi H 2004 *Phys. Rev.* B **70** 134512 on LTO and LTT)

[50] Kumagai K, Nakamura Y, Watanabe I, Nakamichi Y and Nakajima H 1988 *J. Magn. Magn. Mater.* **76/77** 601

[51] Bianconi A, Saini N L, Lanzara A, Missori M, Rossetti T, Oyanagi H, Yamaguchi H, Oka K and Ito T 1996 *Phys. Rev. Lett.* **76** 3412

[52a] Withers R L and Wilson J A 1986 *J. Phys. C: Solid State Phys.* **19** 4809

[52b] Fung K K, McKernan S, Steeds J W and Wilson J A 1981 *J. Phys. C: Solid State Phys.* **14** 5417

[53] Yamada K *et al* 1998 *Phys. Rev.* B **57** 6165

[54] Wilson J A, DiSalvo F J and Mahajan S 1975 *Adv. Phys.* **24** 117

[55] Ghazi M E, Spencer P D, Wilkins S B, Hatton P D, Mannix D, Prabhakaran D, Boothroyd A T and Cheong S-W 2004 *Phys. Rev.* B **70** 144507

[56] Colaitis D, van Dyck D, Delavignette P and Amelinckx S 1980 *Phys. Status Solidi* a **58** 271

[57] Billinge S J L, Božin E S, Gutmann M and Takagi H 2000 *J. Supercond.* **13** 713

[58] Gilardi R, Hiess A, Momono N, Oda M, Ido M and Mesot J 2004 *Europhys. Lett.* **66** 840

[59] Niemöller T, Ichikawa N, Frello T, Hunnefeld H, Andersen N H, Uchida S, Schneider J R and Tranquada J M 1999 *Eur. Phys. J.* B **12** 509

see also 1999 *J. Low Temp. Phys.* **117** 455

[60] Hunt A W, Singer P M, Thurber K R and Imai T 1999 *Phys. Rev. Lett.* **82** 4300

[61] Chiba K, Goto T, Mori M, Suzuki T, Seki K and Fukase T 1999 *J. Low Temp. Phys.* **117** 479

[62] Thio T, Thurston T R, Preyer N W, Picone P J, Kastner M A, Janssen H P, Gabbe D R, Chen C Y, Birgeneau R J and Aharony A 1988 *Phys. Rev.* B **38** 905
[63] Issacs E D, Aeppli G, Zschack P, Cheong S-W, Williams H and Buttrey D J 1994 *Phys. Rev. Lett.* **72** 3421
[64] Thurston T R, Gehring P M, Shirane G, Birgeneau R J, Kastner M A, Endoh Y, Matsuda M, Yamada K, Koijima H and Tanaka I 1992 *Phys. Rev.* B **46** 9128
Mason T E, Aeppli G and Mook H A 1992 *Phys. Rev. Lett.* **68** 1414
[65] Kotliar G, Savrasov S Y, Palsson G and Biroli G 2001 *Phys. Rev. Lett.* **87** 186401
Maier T, Jarrell M, Pruschke T and Hettler M H 2005 *Rev. Mod. Phys.* at press
(Maier T, Jarrell M, Pruschke T and Hettler M H 2004 *Preprint* cond-mat/0404055)
Keller M, Metzner W and Schollwöck U 2002 *J. Low Temp. Phys.* **126** 961
[66] Wilson J A 2004 *Preprint* cond-mat/0408037
[67] Quintanilla J and Gyorffy B L 2002 *J. Phys.: Condens. Matter* **14** 6591
Quintanilla J and Gyorffy B L 2003 *Preprint* cond-mat/0304462
[68] Komiya S, Chen H-D, Zhang S-C and Ando Y 2004 *Preprint* cond-mat/0408483
[69] Wakimoto S, Zhang H, Yamada K, Swainson I, Kim H and Birgeneau R J 2004 *Phys. Rev. Lett.* **92** 217004
[70] Wakimoto S, Tranquada J M, Ono T, Kojima K M, Uchida S, Lee S-H, Gehring P M and Birgeneau R J 2001 *Preprint* cond-mat/0103135
[71] Ando Y, Boebinger G S, Passner A, Kimura T and Kishio K 1995 *Phys. Rev. Lett.* **75** 4662
Ando Y, Boebinger G S, Passner A, Wang N L, Geibel C and Steglich F 1996 *Phys. Rev. Lett.* **77** 2065
[72] Komiya S and Ando Y 2004 *Preprint* cond-mat0408627
[73] Vershinin M, Misra S, Ono S, Abe Y, Ando Y and Yazdani A 2004 *Science* **303** 1995
[74] Renner Ch, Revaz B, Kadowaki K, Maggio-Aprile I and Fischer Ø 1998 *Phys. Rev. Lett.* **80** 3606
[75] Hoffman J E, Hudson E W, Lang K M, Madhavan V, Eisaki H, Uchida S and Davis J C 2002 *Science* **295** 466
[76] Hoffman J E, McElroy K, Lee D-H, Lang K M, Eisaki H, Uchida S and Davis J C 2002 *Science* **297** 1148
[77] McElroy K, Lee D-H, Hoffman J E, Lang K M, Lee J, Hudson E W, Eisaki H, Uchida S and Davis J C 2004 *Preprint* cond-mat/0406491
[78] Hanaguri T, Lupien C, Kohsaka Y, Lee D-H, Azuma M, Takano M, Takagi H and Davis J C 2004 *Nature* **430** 1001
[79] Moriya T and Ueda K 2000 *Adv. Phys.* **49** 555
Monthoux P and Lonzarich G 2001 *Phys. Rev.* B **63** 054529
Eremin I, Morr D K, Chubukov A V, Bennemann K and Norman M R 2004 *Preprint* cond-mat/0409599
Manske D, Eremin I and Bennemann K H 2003 *Phys. Rev.* B **67** 134520
Chubukov A V and Norman M R 2004 *Preprint* cond-mat/0402304
[80] Chen H-D, Capponi S, Alet F and Zhang Z-C 2004 *Phys. Rev.* B **70** 024516
Chen H-D, Vafek O, Yazdani A and Zhang S-C 2004 *Preprint* cond-mat/0402323
[81] Fu H C, Davis J C and Lee D-H 2004 *Preprint* cond-mat/0403001
[82] Arrigoni E, Fradkin E and Kivelson S A 2004 *Phys. Rev.* B **69** 214519
[83] Balents L, Bartosch L, Burkov A, Sachdev S and Sengupta K 2004 *Preprint* cond-mat/0408329
[84] Melikyan A and Tesanovic Z 2004 *Preprint* cond-mat/0408344
[85] Huang H-X, Li Y-Q and Zhang F-C 2004 *Preprint* cond-mat/0408504
[86] Derzhko V and Jedrzejewski J 2004 *Preprint* cond-mat/0409044
[87] Franz M 2004 *Preprint* cond-mat/0409431
[88] Norman M R, McMullan G J, Novikov D L and Freeman A J 1993 *Phys. Rev.* B **48** 9935 [LSCO]
[89] Novikov D L and Freeman A J 1993 *Physica* C **212** 233
Novikov D L and Freeman A J 1993 *Physica* C **216** 273 [Hg-1201]
[90] Singh D J and Pickett W E 1992 *Physica* C **203** 193 [Tl-2201]
[91] Kim T K, Kordyuk A A, Borisenko S V, Koitzsch A, Knupfer M, Berger H and Fink J 2003 *Phys. Rev. Lett.* **91** 167002
[92] Gofron K, Campuzano J C, Abrikosov A A, Lindros M, Bansil A, Ding H, Koelling D and Dabrowski B 1994 *Phys. Rev. Lett.* **73** 3302
[93] King D M, Shen Z-X, Dessau D S, Marshall D S, Park C H, Spicer W E, Peng J L, Li Z Y and Greene R L 1994 *Phys. Rev. Lett.* **73** 3298
[94] Ma J, Alméras P, Kelley R J, Berger H, Margaritondo G, Cai X Y, Feng Y and Onellion M 1995 *Phys. Rev.* B **51** 9271
[95] Norman M R, Ding H, Randeria M, Campuzano J C, Yokoya T, Takeuchi T, Mochiku T, Kadowaki K, Guptasarma P and Hinks D G 1998 *Nature* **392** 157
Norman M R, Ding H, Campuzano J C, Takeuchi T, Randeria M, Yokoya T, Takahashi T, Mochiku T and Kadowaki K 1997 *Phys. Rev. Lett.* **79** 3506

[96] Takagi H, Batlogg B, Kao H L, Kwo J, Cava R J, Krajewski J J and Peck W F Jr 1992 *Phys. Rev. Lett.* **69** 2975
[97] McKenzie A P, Hughes D, Cooper J R, Carrington A, Chen C and Wanklyn B M 1992 *Phys. Rev.* B **45** 527
Carrington A, Colson D, Dumont Y, Ayache C, Bertinoti A and Manacco J F 1994 *Physica* C **234** 1
[98] Parker I D and Friend R H 1988 *J. Phys. C: Solid State Phys.* **21** L345
[99] Obertelli S D, Cooper J R and Tallon J L 1992 *Phys. Rev.* B **46** 14928
[100] Khodel V A, Clark J W and Shaginyan V R 1995 *Solid State Commun.* **96** 353
Khodel V A, Shaginyan V R and Khodel V V 1994 *Phys. Rep.* **249** 1
Khodel V A, Shaginyan V R and Shuk P 1996 *JETP Lett.* **63** 651
Zverev M V, Khodel V A and Clark J W 2001 *JETP Lett.* **77** 46
Khodel V A and Yakovenko V M 2003 *JETP Lett.* **77** 420
Clark J W, Khodel V A, Zverev M V and Yakavenko V M 2004 *Phys. Rep.* **391** 123
[101] Civelli M, Capone M, Kancharla S S, Parcollet O and Kotliar G 2004 *Preprint* cond-mat/0411696
[102] Carter E C and Schofield A J 2004 *Phys. Rev.* B **70** 045107
[103] Tanaka K *et al* 2004 *Phys. Rev.* B **70** 092503
[104] Ronning F *et al* 2003 *Phys. Rev.* B **67** 165101
[105] Tohyama T and Maekawa S 2003 *Phys. Rev.* B **59** 092509
[106] Ino A, Kim C, Nakamura M, Yoshida T, Mizokawa T, Fujimori A, Shen Z-X, Kakeshita T, Eisaki H and Uchida S 2002 *Phys. Rev.* B **65** 094504
[107] Hussey N E, Takenaka K and Takagi H 2004 *Phil. Mag.* **84** 2847
[108] Matsuzaki T, Monomo N, Odo M and Ido M 2004 *Preprint* cond-mat/0408606
[109] Hwang H Y, Batlogg B, Takagi H, Kao H L, Kwo J, Cava R J, Krajewski J J and Peck W F 1994 *Phys. Rev. Lett.* **72** 2636
Ando Y, Kurita Y, Komiya S, Ono S and Segawa K 2004 *Phys. Rev. Lett.* **92** 197001
[110] Fujita S, Obata T, Morabito D L and Shane T F 2000 *Phys. Rev.* B **63** 054402
[111] Nakamae S, Behnia K, Mangkorntong N, Nohara M, Takagi H, Yates S J C and Hussey N E 2003 *Phys. Rev.* B **68** 100502(R)
[112] Chen Q, Levin K and Kosztin I 2001 *Phys. Rev.* B **63** 184519
Gyorffy B L, Staunton J B and Stocks G M 1991 *Phys. Rev.* B **44** 5190
[113] Christensen N B, McMorrow D F, Rønnow H M, Lake B, Hayden S M, Aeppli G, Perring T P, Mangkorntong M, Nohara M and Takagi H 2004 *Phys. Rev. Lett.* **93** 147002
[114] Stock C, Buyers W J L, Liang R, Peets D, Tun Z, Bonn D, Hardy W N and Birgeneau R J 2004 *Phys. Rev.* B **69** 014502
Stock C *et al* 2004 *Preprint* cond-mat/0408071
Pailhès S, Sidis Y, Bourges P, Hinkov V, Ivanov A, Ulrich C, Regnault J P and Keimer B 2004 *Phys. Rev. Lett.* **93** 167001
Hinkov V, Pailhès S, Bourges P, Sidis Y, Ivanov A, Kulakov A, Lin C T, Chen D P, Bernhard C and Keimer B 2004 *Nature* **430** 650
[115] Li Y and Lieber C M 1993 *Mod. Phys. Lett.* B **7** 143
[116] Johnson P D *et al* 2001 *Phys. Rev. Lett.* **87** 177007
[117] Chubukov A V, Jankó B and Tchernyshyov O 2001 *Phys. Rev.* B **63** 180507R